Shoreface-connected sand ridges strongly affect decadal shoreline evolution

An idealized modeling study

J.M. Boersma
Master Thesis
Institute for Marine and Atmospheric Research

Utrecht University

Supervisors: prof. dr. H.E. de Swart & dr. A. Nnafie
Second supervisor: prof. dr. L.R.M. Maas

Student number: 7001606
April 2023

Abstract

It is well known that climate change has a potentially strong impact on the evolution of shorelines and adjacent coastal waters at decadal timescales. This study focuses on a different driver of decadal coastal evolution that acts on several coasts (e.g. that of Belgium) due to the presence of shoreface-connected ridges on the shelf. These are bedforms with a scale of several kilometers and crests that are obliquely oriented to the coastline. Previous work has shown that such ridges cause focusing and defocusing of energy of incoming waves, thereby resulting in gradients in the longshore wave-driven sand transport along the coast. Extending that earlier work, the present research quantifies the dependence of the response of the shoreline (mean position, variability in position, location of erosional hotspots) to shoreface-connected ridges with different orientations and positions with respect to the shoreline. Moreover, the dependence of the shoreline response to the characteristics of the wave climate (fixed direction versus variable directions) is assessed. This is done by forcing a morphodynamic, non-linear shoreline model (Q2Dmorfo) with waves obtained from a morphostatic shelf model (Delft3D + SWAN). The latter computes wave propagation on an idealized shelf bathymetry in the presence of tides. The model results for parameter values representative of the Belgian coast, and shelf indicate that accumulation (erosional) hotspots form near crests (troughs). Furthermore, the closer the ridges and the larger the angle with the coast, the stronger these hotspots are. The locations of these hotspots vary for different offshore distances and ridge orientations. If the incoming waves have variable heights and directions, it turns out that the location of the hotspots remains the same, their magnitude is two times smaller, and the increase in mean shoreline position is four times as small. The results suggest a nourishing effect of onshore propagating ridges, although smaller than current rates of sea level rise. The results qualitatively agree with observations, although the growth rate and absolute magnitude exceed realistic conditions.

Contents

1 | Introduction

This thesis considers the shoreline dynamics on decadal times scales influenced by shoreface-connected sand ridges. The introduction consists of four main sections. In Section 1.1, the general geographical and physical context is described. Section 1.2 explains the importance of the research topic, while Section 1.3 presents the current state of understanding. Finally, Section 1.4 outlines the aims of the thesis, as well as the approach that is taken to achieve these goals.

1.1 The coastal zone

The coastal zone is a body of water that spans from the shoreline to the shelf break, where the seafloor undergoes a large slope towards the deep ocean (Figure 1.1). The coastal zone comprises several distinct areas. The nearshore zone, which is the focus of this thesis, extends from the shoreline to the wave base, where waves interact with the seabed under average wave conditions, marking the transition to the inner shelf. The nearshore zone has a steep transverse bottom slope (of the order of $\sim 10^2$ m/m), while the inner shelf has a smaller sloping bottom, typically around $\sim 10^3$ m/m, which becomes even smaller on the outer shelf.

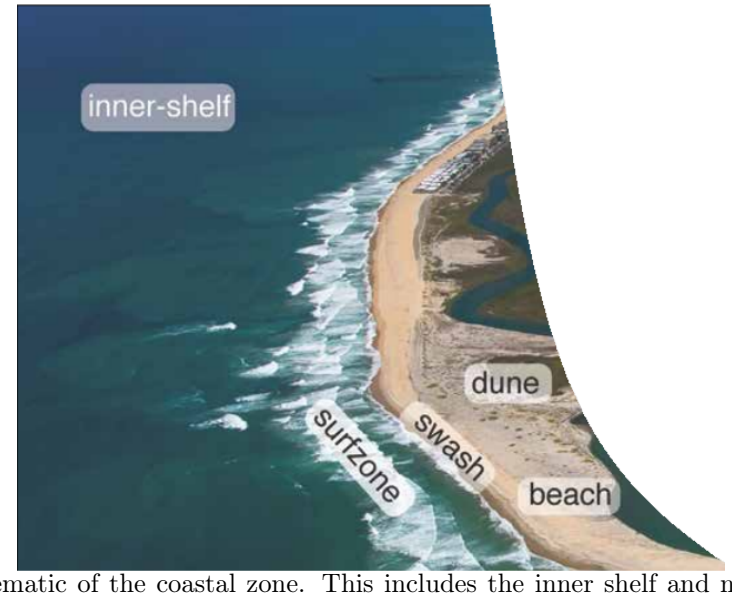

Figure 1.1: Schematic of the coastal zone. This includes the inner shelf and nearshore, where the latter comprises the surf zone, swash zone, beach, and dunes. Adapted from Elko et al. (2015).

The nearshore zone is a complex and dynamic environment where numerous phenomena occur at different times and length scales. Within the nearshore zone, three subzones are distinguished: the swash zone, surf zone, and shoaling zone (Figures 1.1and 1.3). The most important processes in the shoaling zone, which extends from the wave base to the point where waves break, are associated with the shoaling (increasing of wave height) and refraction (changing of wave direction) of wind-generated sea waves as they move towards the shore. The surf zone extends from the shoreline to the point where waves break, known as the breaker zone. Waves continuously stir up material from the seabed, which is then transported by the longshore current generated by the breaking of waves in the surf zone. Sediment is transported along the coast between the depth of closure and the shoreline by this wave-driven current in a process known as littoral drift.

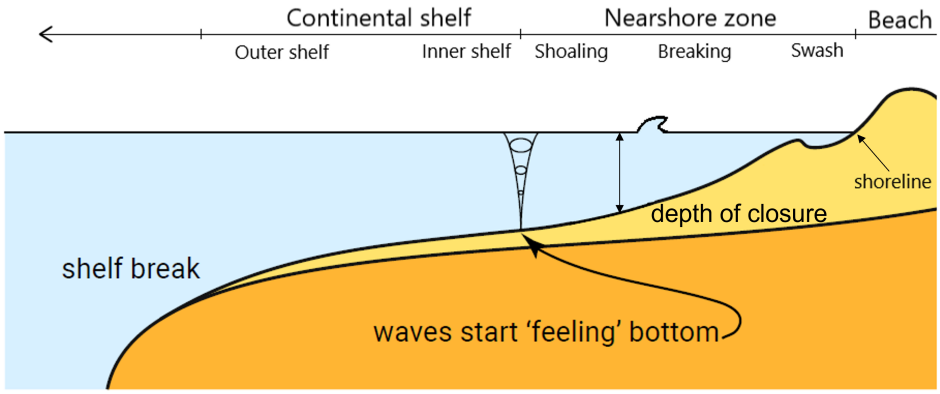

Figure 1.2: An idealized cross-shore section, adapted from Bosboom and Stive (2021).

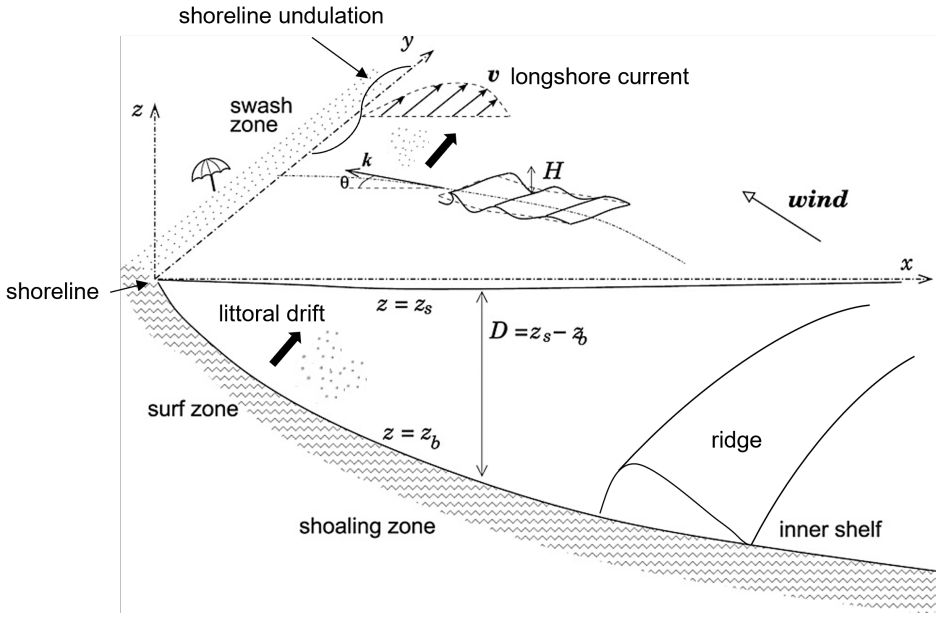

Figure 1.3: Schematic drawing of the coastal system and the four zones considered in this thesis. The swash, surf, and shoaling zones are subzones of the nearshore zone and are separated from the inner shelf by the wave base. The depth of closure is the seaward end of the zone where most sediment transport is found. See also Figure 1.2. Some important processes are visualized, such as shoaling, refraction, wave breaking, longshore currents, and littoral drift. A ridge is located on the inner shelf. Adapted from Ribas et al. (2015).

Changes in the shape, or morphology, of the coastal zone occur when the rate of sediment transported into a certain area is not balanced by the sediment leaving that area. This results in a gradient in longshore transport, causing erosion in the direction of the positive transport gradient and accretion in the direction of the negative transport gradient. However, as the morphology changes, the waves and tides, dependent on the water depth, respond to the adjusted bed level, resulting in changes in sediment transport rates. In turn, this affects the development of the morphology. This feedback between hydrodynamic processes and morphology, or morphodynamics, can be either stabilizing or destabilizing. The morphodynamic feedback is shown in Figure 1.4.

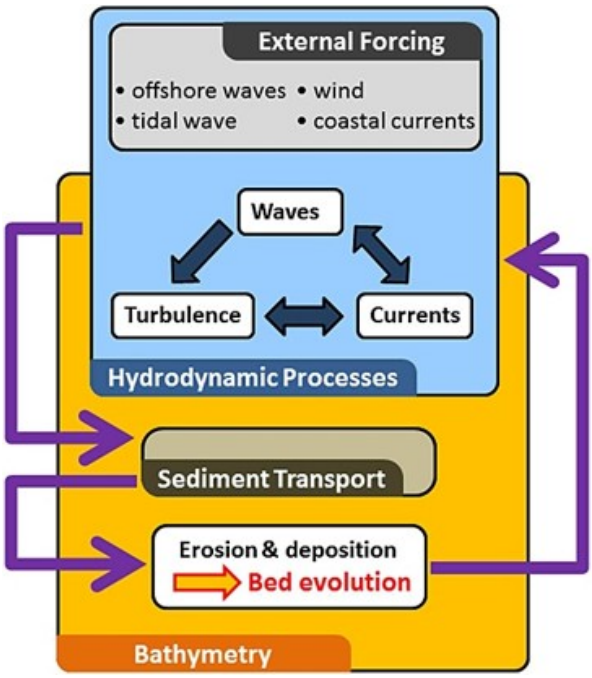

Figure 1.4: Sketch of the general framework of coastal morphodynamic models. Hydrodynamic processes influence sediment transport, which influences bed evolution. In turn, this influences the hydrodynamic processes again. Adopted from Ribas et al. (2015)

Undulations of the bed and shoreline that emerge due to this morphodynamic feedback are an integral part of the coastal system. In the nearshore zone, small-scale bedforms such as ripples and sandbars and shoreline undulations such as beach cusps can be found in the nearshore zone. They typically have spatial scales of centimeters to hundreds of meters and change at timescales of hours to years. Bedforms with larger spatial and time scales than those in the nearshore zone are found further offshore with scales on the order of kilometers and time scales ranging from decades to centuries. Examples are tidal sand ridges on the outer shelf and shoreface-connected sand ridges on the inner shelf (Figure 1.5and 1.7). These are elongated sandy bodies spanning a few kilometers and change on timescales of decades to centuries. The ridges are oriented at an angle relative to the shoreline and are separated by a consistent distance in the alongshore direction (Dyer and Huntley, 1999, and references therein). These features play a role in the evolution of the coastal zone, as will be explained later.

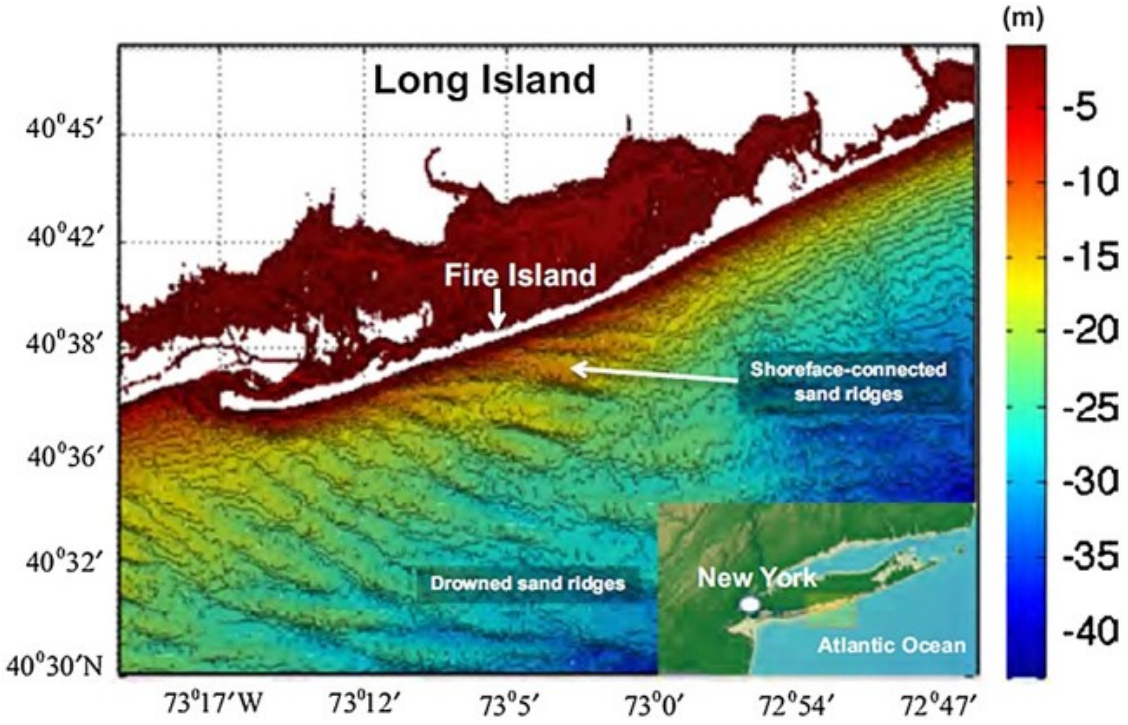

Figure 1.5: Bathymetrical map showing the shoreface-connected ridges located at the coast of Long Island on the US Atlantic coast. The spacing between the ridges is approximately 1-2 kilometers. Adopted from Nnafie (2014).

1.2 Relevance

The natural beauty, recreational opportunities, and economic benefits coastal zones provide make them highly valued worldwide. Consequently, over half of the world's population has settled along this narrow strip, with this proportion continuing to rise (Komar, 1998), and the preservation of coastal zones has become crucial for social, economic, and ecological reasons. Coastal evolution is a major concern for many communities around the world. Particularly, changes in the position of the shoreline can lead to the loss of valuable property and infrastructure and the degradation of natural habitats. To mitigate and adapt to this threat, it is crucial to understand the regional morphology that impacts shoreline evolution. Many of such coasts' changes are generally attributed to increased rates of local sea-level rise (Pörtner et al., 2022). However, erosion and accretion rates are highly variable in both space and time because of two reasons. First, engineering works (harbors, hard protection structures) cause local erosion-deposition patterns at the same scale as that of the measure (Szmytkiewicz et al., 2000). Second, the bathymetry of coastal areas is highly irregular and dynamic. In particular, large sand ridges on the inner shelf cause wave energy focusing, affecting the morphodynamics of the nearshore zone and its shoreline (Safak et al., 2017; Nnafie et al., 2021). With current-day nourishment frequencies of $\sim 5 - 20$ years (Roest, 2022), efficient coastal management strategies require a good understanding of the morphodynamics of the shoreline at decadal timescales. In the following section, the current state of research concerning shoreline evolution is briefly discussed.

1.3 Current understanding

Traditionally, shoreline evolution has been approached from an equilibrium perspective. Early approaches predict shoreline change due to interrupted longshore transport using a diffusion-type equation based on the assumptions of a small angle of incidence and a constant cross-shore profile shape (Pelnard-Considere, 1956). Later, these standard 1D models also incorporated more advanced physics to estimate transport rate as a function of wave conditions, sediment properties, and profile shape (e.g. Hanson (1989), Tonnon et al. (2018)). However, these models still assume that the sediment transport depends on the wave angle in a sinusoidal way, with a maximum at roughly 45° of incoming wave angle, beyond which the shoreline becomes fundamentally unstable.

When the direction of incoming waves exceeds this angle, large shoreline undulations emerge as free instabilities, which occur when a system evolves from an unstable equilibrium morphology to another without external intervention. This is the case for high-angle wave instability (HAWI). Ashton et al. (2001) showed that a straight sandy shoreline could develop undulations with lengthscales in the kilometer range, known as large-scale shoreline sand waves when the wave angle surpasses a critical angle θ_c (about 42°) in deep water (before wave refraction and shoaling). Later research (Falqués and Calvete, 2005; Ashton and Murray, 2006; van den Berg et al., 2011; Falqués et al., 2017), indicated that the value of θ_c differs based on the wave properties, the nearshore bathymetry profile, and the depth of closure D_c. These analyses revealed that the refraction in the nearshore zone near shoreline undulations is important and generally leads to shoreline stabilization relative to the original HAWI mechanism proposed by Ashton et al. (2001). Here Falqués et al. (2017) also included low-angle wave instability (LAWI) of the shoreline, which can develop in case of steep beaches and relatively small wave heights as shown by Idier et al. (2011). The developed idealized shoreline models have been used to successfully model the decadal evolution of shoreline sand waves and mega nourishments as present at the Dutch coast (Van den Berg et al., 2012; Arriaga et al., 2017; Falqués et al., 2017). In these studies, the undulations evolve due to morphodynamic feedback and self-organization see Figure 1.6a. However, this is not the only mechanism that can explain patterns in the coastal zone. Instead of morphodynamic self-organization, undulations can develop due to variations in external forcing due to a certain template for the hydrodynamics or morphology. Templates refer to pre-existing spatially organized structures in the hydrodynamics or the underlying geology, whose shape would be imprinted on unconsolidated sand(Coco and Murray, 2007). This is visualized in Figure 1.6b.

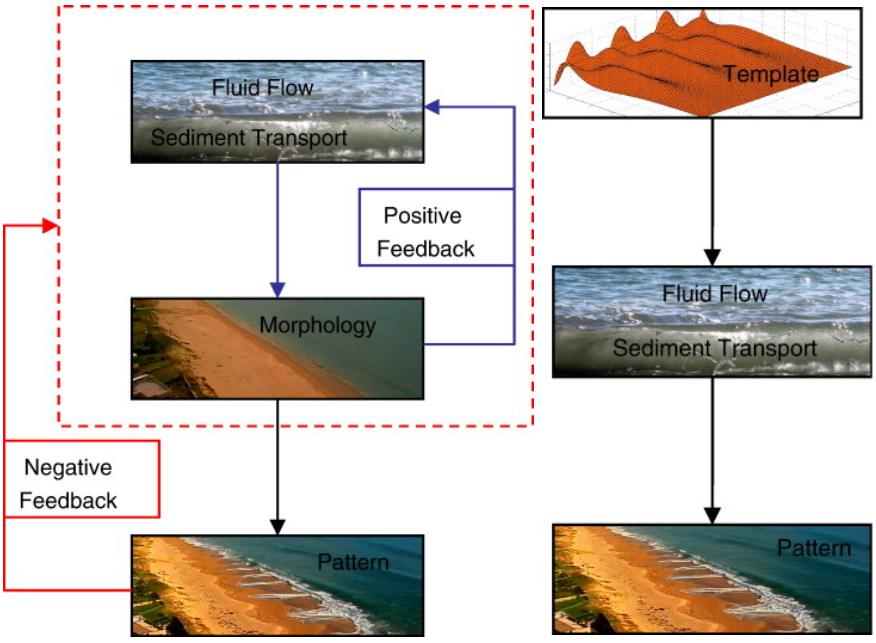

(a) Self-organization **(b)** Forcing template

Figure 1.6: Schematic overview of morphodynamic self-organization (a) versus the concept of forcing templates (b). Adopted from Coco and Murray (2007)

An example of morphological development due to forcing templates is the influence of offshore located outer bars on inner bar rip channel development. This Castelle et al. (2010) showed that the outer bars acted as a forcing template for developing the inner bars by focussing and defocussing wave energy. Other bedforms are known to act as forcing templates too. In particular, large sand ridges on the inner shelf cause focusing of wave energy, which affects the morphodynamics of the nearshore zone and its shoreline (Safak et al., 2017; Nnafie et al., 2021). An example of those bedforms is shoreface-connected sand ridges, which have been recognized to cause undulations of the adjacent shoreline of Fire Island (USA) (Schwab et al., 2000). Through a model that accounts for three-dimensional flow, waves, and sediment transport, Safak et al. (2017) demonstrated that the effects of SFCR on nearshore flow and sediment transport processes control the shoreline undulations, meaning that the longshore spacings of these bottom features are imprinted on the shoreline morphology. This shows that shoreline undulations can be forced by ridges on the shelf rather than being self-organizing patterns due to free instabilities, e.g., incoming (high-angle) waves. Nnafie et al. (2021) further investigated this shelf-shoreline coupling for the shoreface connected ridges along the coast of Fire Island. They demonstrate that significant coupled behavior between the shelf ridges and the shoreline undulations occurs when wave propagation is predominantly aligned with the long axis of the ridges. This can lead to prominent shoreline undulations that affect the shelf morphology, with the longshore spacing of the ridges strongly imprinted on the shoreline morphology.

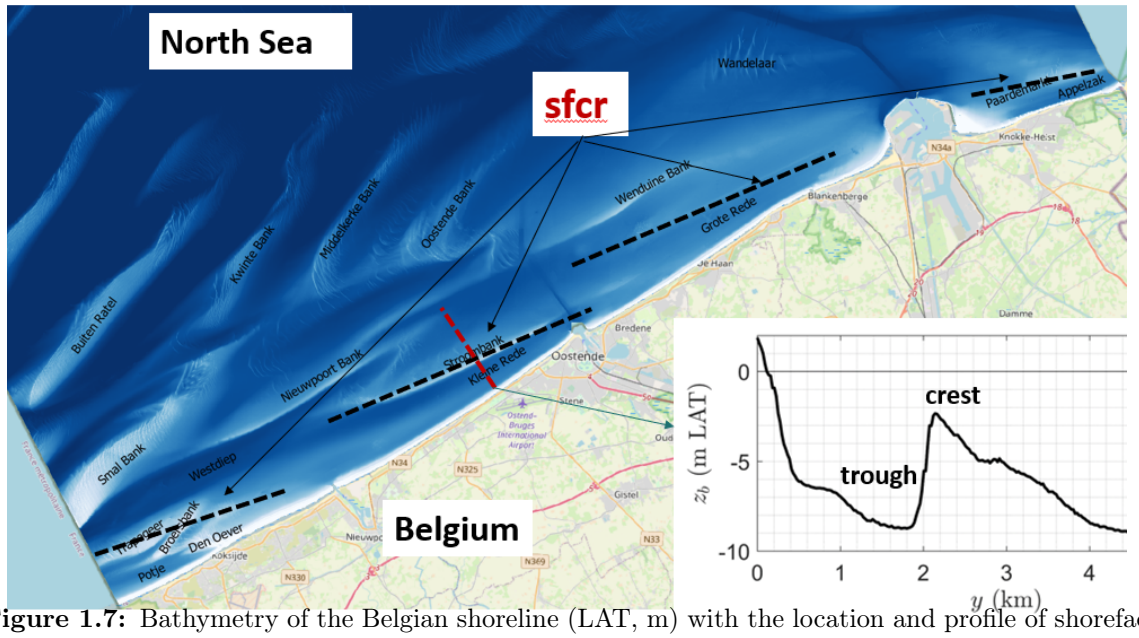

Figure 1.7: Bathymetry of the Belgian shoreline (LAT, m) with the location and profile of shoreface connected ridges (SFCR). The red dotted line indicates the location of the cross-shore profile of the Stroombank SFCR.

Shoreline sand waves have been observed but are not considered persistent since their lifetimes are shorter than those of the ridges (Ruessink and Jeuken, 2002). In several other shelf-shoreline systems, however, such as the Belgian coast (see Figure 1.7) and the central Dutch coast, large-scale shoreline undulations are not observed despite the presence of much larger sand ridges on their shelves. This raises the question of why the forcing template of large ridges on the inner shelf does not always lead to persistent shoreline undulations. A possible explanation could lie in the different environmental conditions of the systems. As of now, research has focused on shoreface-connected ridges, which are rather oblique, are present at a considerable distance to the coast, and local hydrodynamic conditions are microtidal and a unidirectional wave climate (Safak et al., 2017; Nnafie et al., 2021). In contrast, the dynamics of coasts featuring significant tides, a bi-directional wave climate, and almost shore parallel, onshore-located sand ridges (Figure 1.7) are poorly understood, and a fundamental understanding of the link between these different conditions and the observed differences in shoreline evolution is yet to be obtained.

1.4 Aims and Approach

Based on the knowledge gaps identified, this research aims to expand our understanding of the impact of a bi-directional wave climate and almost shore parallel, onshore located, and onshore migrating sand ridges to decadal shoreline evolution in the presence of significant tides. This leads to the following research questions:

1. What are the differences in tidal currents, wave patterns, sediment transport, and evolution of the shoreline between the case that ridges on the shelf are absent, respectively present?

2. What is the influence of the characteristics (location and orientation) of almost shore parallel, onshore-located sand ridges on the decadal shoreline evolution?

3. What is the influence of wave direction and variation in wave conditions in the presence of almost shore parallel, onshore-located sand ridges on decadal shoreline evolution?

This research focuses on determining the strength and location of accretion and erosion hotspots, as these features are most pressingly impacting coastal management strategies. An idealized numerical modeling study is conducted to improve the fundamental understanding of shoreline dynamics in the conditions described above. There are several reasons for this choice. An idealized numerical model is fast, keeping computation times manageable and allowing one to focus on critical processes. To address the research questions, the method of Nnafie et al. (2021) is adapted for specific circumstances. This unique model pairs a high-performance shelf model with a non-linear, morphodynamic shoreline model to resolve the processes relevant to decadal timescales in the nearshore zone.

The model used in this research is explained in Section 2, containing the structure, configuration, and experimental setup used to answer the research questions. The results of the experiments are discussed in Section 3 and discussed in Section 4. Section 5 contains the conclusions and answers to the research questions.

2 | Model and Methods

This project uses an idealized numerical modeling approach based on the method of Nnafie et al. (2021). Decadal shoreline evolution is simulated by forcing a morphodynamic, non-linear shoreline model (Q2Dmorfo) with waves obtained from a morphostatic shelf model (Delft3D + SWAN). The latter computes wave propagation on an idealized shelf bathymetry in the presence of tides. The physical model is described in Section 2.1, and Section 2.2 contains the numerical aspects, after which the setup of experiments is described in Section 2.3. The analysis of the output is briefly described in Section 2.4.

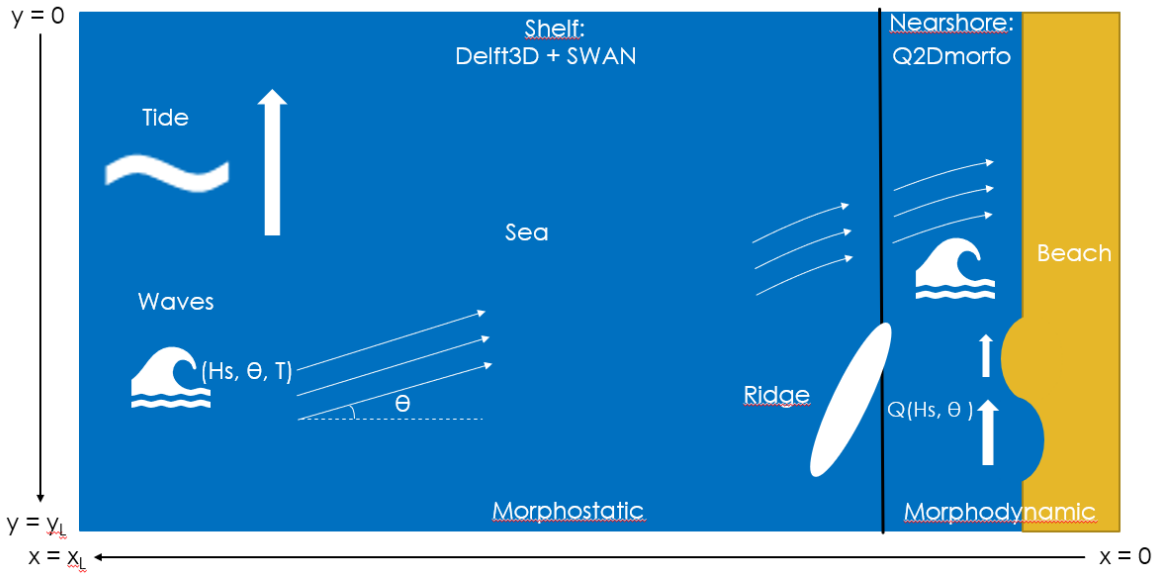

Figure 2.1: Overview of the coupled shelf-shoreline system. The Cartesian coordinate system is defined with the positive x-axis directed seaward (from $x_0 = 0$ to (x_L)), and the positive y-axis is directed north to south (from $y_0 = 0$ to (y_L)).

2.1 Physical Model

2.1.1 Domain

A simplified model of a coastal region is used, comprising two rectangular areas representing the shelf and nearshore. A schematic overview is given in Figure 2.1. A Cartesian coordinate system is defined with the positive x-axis directed seaward (from $x_0 = 0$ to x_L), and the positive y-axis is directed north to south (from $y_0 = 0$ to y_L). The shelf area is defined by the coordinates x_1 to x_L and y_0 to y_L, while the nearshore area is defined by the coordinates x_0 to x_2 and y_0 to y_L. The nearshore area is further divided into two sections: a dry area (beach) located between x_0 and x_s, and a wet area between x_s and x_2. The position of the shoreline, represented by x_s, is allowed to change, with the dry area experiencing erosion or accretion. On the shelf, currents and waves are resolved on a bathymetry that does not change in time, i.e. a morphostatic bed, in the presence of tides. This serves to compute the hydrodynamic boundary conditions for the nearshore zone, which are used to simulate the evolution of the shoreline x_s.

The base topography of the coupled shelf-shoreline system is assumed to have a mean depth, H_1, that depends on the cross-shore coordinate x. In the nearshore dry area ($0 \leq x \leq x_{s0}$), the height decreases from b at the landward end to 0 at the shoreline, with a slope determined by the parameter β. Between $xs0$ and x_2, including the coupling zone between x_1 and x_2, a modified Dean equilibrium beach profile is used, with a constant α determined by Equation A.2 (Appendix)(Figure 2.2b). Offshore of x_2, the depth $H(x)$ varies linearly from $H1$ at$x = x_2$ to H_2 at $x = x_L$ (Figure 2.2a). This type of shelf bathymetry has been used in previous studies (Nnafie et al., 2020, 2021; Tao et al., 2019) and is supported by field data (Hamon-Kerivel et al., 2020).

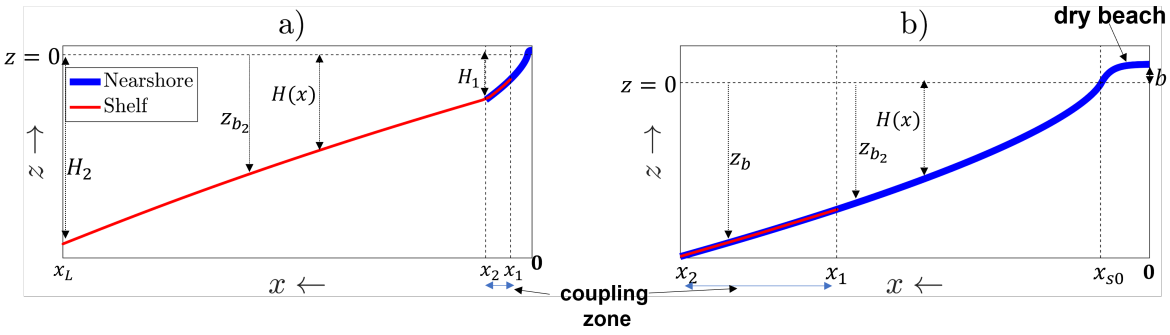

Figure 2.2: The cross-shore profile of the mean depth $H(x)$ of the coupled shelf-shoreline modeling system is shown in panel (a) and described by Equation A.1. The system consists of a dry beach ($0 \leq x \leq xs0$) with height gradually decreasing from b at $x = 0$ to 0 at $x = x_{s0}$. In the region $x_{s0} \leq x \leq x_2$, which includes the coupling zone between x_1 and x_2, the depth $H(x)$ follows a shifted Dean equilibrium profile. Further offshore, $H(x)$ increases linearly from H_1 at $x = x_2$ to H_2 at the seaward boundary (xL). A zoom-in of the region between 0 and x_2 is displayed in panel (c). Adapted from Nnafie et al. (2021).

2.1.2 Currents

The non-linear depth-averaged shallow water equations describe the currents on the shelf s:

$$\frac{\partial \eta}{\partial t} + \frac{\partial (Du)}{\partial x} + \frac{\partial (Dv)}{\partial y} = 0, \tag{2.1a}$$

$$\frac{\partial u}{\partial t} + u\frac{\partial u}{\partial x} + v\frac{\partial u}{\partial y} - fv = -g\frac{\partial \eta}{\partial x} - \frac{\tau_x}{\rho D} + \frac{\nu}{D}\left[\frac{\partial}{\partial x}\left(D\frac{\partial u}{\partial x}\right) + \frac{\partial}{\partial y}\left(D\frac{\partial u}{\partial y}\right)\right] + \frac{1}{\rho D}F_x, \tag{2.1b}$$

$$\frac{\partial v}{\partial t} + u\frac{\partial v}{\partial x} + v\frac{\partial v}{\partial y} + fu = -g\frac{\partial \eta}{\partial y} - \frac{\tau_y}{\rho D} + \frac{\nu}{D}\left[\frac{\partial}{\partial x}\left(D\frac{\partial v}{\partial x}\right) + \frac{\partial}{\partial y}\left(D\frac{\partial v}{\partial y}\right)\right] + \frac{1}{\rho D}F_y, \tag{2.1c}$$

In these equations, t represents time, η represents the sea surface elevation relative to the mean sea level ($z = 0$), and D is the water depth measured from the bed level z_b relative to the mean sea level. The variables u and v represent the cross and longshore components of depth-averaged velocity $\mathbf{v}$, respectively. The parameter f represents the Coriolis parameter, and g represents the gravitational acceleration. The variables τ_x and τ_y represent the bed shear stress components, which result from the combined effect of currents and waves (Soulsby et al., 1993) and next to the current velocity magnitude U and depth z_b, it is dependent on the angle between the current direction and the direction of wave propagation θ, significant wave height H_s, and wave period T (see next section). ρ represents the density of water, ν the horizontal eddy viscosity. The variables F_x and F_y represent the respective components of the wave-induced force per surface area, which are calculated from the divergence of the radiation stress tensor $\bar{\bar{S}}$ (Longuet-Higgins and Stewart, 1964) by

$$F_x = -\left[\frac{\partial S_{xx}}{\partial x} + \frac{\partial S_{xy}}{\partial y}\right], \tag{2.2}$$

$$F_y = -\left[\frac{\partial S_{yx}}{\partial x} + \frac{\partial S_{yy}}{\partial y}\right]. \tag{2.3}$$

In turn, the elements of the radiation stress tensor $\bar{\bar{S}}$ (S_{xx},S_{xy}, S_{yx}, S_{yy}) are the depth-integrated, phase-averaged, excess momentum fluxes of surface gravity waves (see next section). Neumann-type boundary conditions as oscillating water-level gradients are applied at the lateral boundaries to prescribe gradients in the water-level variations. A tidal wave is set to propagate in the negative y-direction and is imposed along the seaward boundary $x = x_L$, following the procedure suggested by Roelvink and Walstra (2004). This is done by prescribing a M_2 water level with amplitude ζ_{M_2} and phase difference $\Delta\phi_{M_2}$ over the western boundary, between the lateral boundaries $y = 0$ and $y = y_L$ at $x = x_L$.

2.1.3 Waves

The evolution of waves is modeled with the spectral wave action balance, which conserves wave energy in the frequency-directional domain (Holthuijsen, 2007). The (spectral) energy of individual wave packets is not conserved in the presence of mean currents since the transfer of energy between waves and currents is possible, but the (spectral) wave action is conserved. The equation is given by:

$$\nabla \cdot [(\mathbf{c_g} + \mathbf{v})N] + \frac{\partial c_\theta N}{\partial \theta} + \frac{\partial c_\sigma N}{\partial \sigma} = \frac{S_{tot}}{\sigma} \tag{2.4}$$

Here, the spectral action density N and wave frequency σ are related by $N = E/\sigma$, where E is the spectral energy density. It is important to note that σ is the wave frequency relative to the local mean current U, instead of the absolute wave frequency $\omega = \sigma + |\mathbf{k}|U_n$ (U_n is the mean current in the direction of wave propagation). The first term of the balance describes the propagation of the action density in space with a group velocity $\mathbf{c_g} = \partial\sigma/\partial\mathbf{k}$ following the dispersion relation $\sigma^2 = g|\mathbf{k}|\tanh(|\mathbf{k}|D)$, where $\mathbf{k}$ is the wave vector and $|\mathbf{k}|$ is the wave number. The second term accounts for the effect of frequency shifting due to variations in depth and currents. The third term represents the depth and current-induced refraction. The propagation velocities c_σ and c_θ are calculated using linear wave theory. The right-hand term $\frac{S_{tot}}{\sigma}$ represents all processes responsible for generating (such as wind), dissipating (such as whitecapping, bottom friction, and depth-induced breaking), or redistributing wave energy (such as non-linear wave-wave interactions). The dissipation due to whitecapping, bottom friction, and depth-induced breaking are included using the respective formulations of Komen et al. (1984), Battjes and Janssen (1978)), and Hasselmann et al. (1973) (JONSWAP). However, non-linear wave-wave interactions and wave growth through wind are neglected in this study. Radiation stresses S_{xx},S_{xy}, S_{yx}, S_{yy} as defined in SWAN are

$$S_{xx} = \int_0^\infty \int_0^{2\pi} \left(n - \frac{1}{2} + n\cos^2\theta\right) E \, \mathrm{d}\theta\mathrm{d}\sigma, \tag{2.5a}$$

$$S_{xy} = \int_0^\infty \int_0^{2\pi} (n\cos\theta\sin\theta) E \, \mathrm{d}\theta\mathrm{d}\sigma, \tag{2.5b}$$

$$S_{yx} = \int_0^\infty \int_0^{2\pi} (n\sin\theta\cos\theta) E \, \mathrm{d}\theta\mathrm{d}\sigma, \tag{2.5c}$$

$$S_{yy} = \int_0^\infty \int_0^{2\pi} \left(n - \frac{1}{2} + n\sin^2\theta\right) E \, \mathrm{d}\theta\mathrm{d}\sigma, \tag{2.5d}$$

in which $n = c_g/c = \frac{1}{2}\left(1 + \frac{2|\mathbf{k}|(\eta - z_b)}{\sinh 2|\mathbf{k}|z_b}\right)$ is the ratio of the group velocity and phase velocity (Holthuijsen, 2007). The seaward boundaries are imposed with JONSWAP spectra of incoming waves. JONSWAP spectra are distributions of wave energy based on observations, characteristic of wind sea in oceanic waters. Energy is distributed over a band of frequencies and directions of waves. As the distribution has a certain universal shape, the characteristics of this distribution can be captured in a couple of parameters. In this thesis, the waves in the energy density spectrum are characterized by significant wave height H_{s0}, peak period T_{p0}, and wave direction θ_0, defined relative to the negative x-axis (positive counter-clockwise). The peak period T_p is the wave period of the absolute maximum of the wave energy density spectrum. The significant wave height H_s and mean wave direction θ, respectively, relate to the energy density spectrum through

$$H_s = 4\sqrt{\int_0^\infty \int_0^{2\pi} E_(\sigma,\theta)\mathrm{d}\sigma\mathrm{d}\theta}, \tag{2.6}$$

$$\theta_{mean} = \frac{\int_0^\infty \int_0^{2\pi} \sin\theta E_(\sigma,\theta)\mathrm{d}\sigma\mathrm{d}\theta}{\int_0^\infty \int_0^{2\pi} \cos\theta E_(\sigma,\theta)\mathrm{d}\sigma\mathrm{d}\theta}. \tag{2.7}$$

The mathematical formulation of the JONSWAP spectrum and a more elaborate description of waves in coastal and oceanic waters can be found in Holthuijsen (2007).

2.1.4 Nearshore zone

In the nearshore zone, the main interest lies in the processes that affect the evolution of the shoreline on a timescale of years to decades. For this, it is not required to incorporate all complex hydrodynamic processes but rather the processes that affect the equilibrium configuration of the coastline. Following Van den Berg et al. (2012); Arriaga et al. (2017), a non-linear shoreline model (Q2Dmorfo) that predicts the morphodynamic evolution of the nearshore and the changes in shoreline position $x_s(y,t)$ without explicitly resolving the current field is used. Instead, empirical formulations directly calculate sediment transport from the wave field. The significant wave height (H_s), peak period (T_p), and wave direction (θ) are used as boundary conditions at the seaward boundary of the shoreline model, which vary alongshore due to variation of the shelf bed level and wave forcing. Wave propagation is computed using the geometrical optics approximation. Monochromatic waves are assumed, and linear wave theory is used to describe the wave field, which is determined by frequency σ, wavenumber k, angle of incidence θ, and significant wave height H_s. The dispersion relation, equation for wave number irrotationality, and conservation of wave energy density are solved to obtain the wave characteristics, which are, respectively:

$$\sigma^2 = gk\tanh(k|z_b|), \tag{2.8}$$

$$\frac{\partial(k\sin\theta)}{\partial x} + \frac{\partial k\cos\theta}{\partial y} = 0, \tag{2.9}$$

$$\nabla\cdot(\mathbf{c_g}H_s^2) = 0. \tag{2.10}$$

Wave conditions are assumed to adapt to variable boundary conditions instantaneously, and wave energy dissipation due to bottom friction and wave breaking is not accounted for. The omission of wave breaking is due to the empirical sediment transport formulations, which require wave conditions at the breaker point $x = x_b$. These conditions are determined by the wave conditions further offshore $x < x_b$. The location of the breaker point x_b is determined using $z_{b1}(x_b) = -\frac{H_s}{\sqrt{2}\gamma_b}$, where γ_b is the breaker index. The boundary condition at the lateral boundary (up-waves) is established by extending the bathymetry uniformly alongshore for a certain distance. It is then assumed that transformed waves enter through the lateral boundary. The sediment transport induced by waves is considered in a simplified manner. To account for the curvature of the shoreline $x_s(y,t)$ and associated bottom contours, the sediment transport vector $\mathbf{Q}$ is expressed in a local coordinate system x', y'. For this, a normal unit vector $\mathbf{n} = (\cos\phi, -\sin\phi)$ and a tangential vector $\mathbf{t} = (\sin\phi, \cos\phi)$ are defined, with ϕ being the local angle of the shoreline concerning the y-axis. Sediment transport $\mathbf{q_{tot}}$ is decomposed into three components:

$$\mathbf{Q} = \mathbf{q_L} + \mathbf{q_C} + \mathbf{q_D}. \tag{2.11}$$

The longshore transport $\mathbf{q_L}$ is caused by breaking waves and parameterised by

$$\mathbf{q_L} = Q_{CERC}(y')f(x')\hat{t}, \tag{2.12}$$

where Q_{CERC} is the cross-shore integrated sediment transport according to the CERC formula (Komar, 1998),

$$Q_{CERC}(y') = \mu(\frac{H_{s,b}}{\sqrt{2}})^{5/2} \sin[2(\theta_b - \phi)]. \tag{2.13}$$

In this equation, the parameter μ governs the magnitude of the sediment transport rate Q. The variables H_{sb} and θ_b represent the significant wave height and wave angle at the breaker point x_b. Additionally, $f(x')$ is a normalized shape function that redistributes the transport rate Q over an area with a cross-shore width of L:

$$f(x') = \frac{4}{\sqrt{\pi}L^3} x'^2 e^{-(\frac{x'}{L})^2}. \tag{2.14}$$

The shape function $f(x')$ is designed to have a similar profile to typical alongshore current profiles observed in the nearshore. The cross-shore width L, which is dependent on y and t, is determined using $L(y,t) = 0.8L_1(y,t) + L_2$, where $L_1(y,t) = x_b(y,t) - x_s(y,t)$ is the width of the surf zone, and L_2 is the width of the swash zone (assumed to be constant). The second contribution, denoted as $\mathbf{q_C}$, parametrizes the cross-shore transport and is based on the assumption that the cross-shore profile of the actual bed-level z_{b1} of the nearshore adjusts to the Dean equilibrium profile $z_{b1,e} = -H(x)$ on long timescales of order years to decades. $\mathbf{q_C}$ is computed as follows:

$$\mathbf{q_C} = -\gamma_C[\nabla z_{b1} \cdot \mathbf{n} - \nabla z_{b_{1,e}} \cdot \mathbf{n}]\mathbf{n}. \tag{2.15}$$

The cross-shore diffusivity coefficient $-\gamma_C$ is variable in space and time and can be estimated using the expression of momentum mixing. For a more detailed description of the module parameters, please take a look at the Appendix.
The third contribution ($\mathbf{q_D}$) of sediment transport in the TRANSP module is a diffusive transport that flattens bumps caused by breaking waves and helps to prevent numerical instabilities by suppressing small-scale noise. This contribution is computed using the following formula:

$$\mathbf{q_D} = -\gamma_D(\nabla z_{b1} \cdot \mathbf{t})\mathbf{t}, \tag{2.16}$$

with alongshore diffusion coefficient γ_D, which is set equal to the cross-shore diffusion coefficient $\gamma_D = \gamma_C$.
The evolution of bed level z_b is based on spatial gradients in sediment transport and conservation of mass, described by

$$(1-p)\frac{\partial z_b}{\partial t} = -\nabla \cdot \mathbf{Q}. \tag{2.17}$$

The dry beach, ranging from 0 to $x_s(y,t)$, undergoes erosion ($\partial z_{b1}/\partial t < 0$) and/or accretion ($\partial z_{b1}/\partial t > 0$). The position of shoreline $x_s(y,t)$ is calculated by linearly interpolating between the cross-shore locations of the last dry cell and the first wet cell of the nearshore domain.
The significant wave height (H_s), peak period (T_p), and wave direction (θ) are used as boundary conditions at the seaward boundary of the shoreline model, which vary alongshore due to variation of the shelf bed level and wave forcing. The up-waves lateral boundary is defined by uniformly extending the bathymetry for a certain alongshore distance and then transforming the waves in this extended bathymetry. The transformed waves are then assumed to enter

through the lateral boundary. Sediment transport is allowed to enter or exit through the seaward ($x = x2$) and lateral boundaries ($y = 0, yL$), while the cross-shore sediment component of $\mathbf{Q}$ is set to zero ($\mathbf{Q}_x = 0$) at the shoreward boundary ($x = 0$).

2.2 Numerical Aspects

The shelf model is Delft3D (Lesser et al., 2004; Deltares, 2019), which comprises the modules FLOW (for water levels and currents) and SWAN (for waves). The shelf model computes the water level and currents on rectilinear, staggered grids with resolution $\Delta x_2 = \Delta y_2$. The equations are solved using a finite differences approach with a hydrodynamic timestep Δt_2. The simulation of wave propagation on the shelf is performed by Module SWAN using the spectral wave action balance, which is applied in a stationary mode (Booij and Holthuijsen, 1987; Holthuijsen, 2007) on the same grid position, resolution, and timestep. Modules FLOW and SWAN communicate online with a certain communication timestep Δt_c. A more elaborate description of the numerical methods can be found in Deltares (2019).

The nearshore model (Q2Dmorfo) uses an explicit finite difference scheme to solve the governing equations. The model uses a Cartesian frame of reference, where the y-axis is parallel to the mean shoreline and the x-axis is pointing offshore, with a rectangular domain ($0 < x < Lx$, $0 < y < Ly$), Lx and Ly being the cross-shore and the alongshore domain lengths, with x cell grid size, Δx, and y cell grid size, Δy. The model has no hydrodynamic timestep but only a morphodynamic timestep Δt_m. A more elaborate description can be found in the work of Van den Berg et al. (2012) and Arriaga et al. (2017). The overall structure of the shelf and shoreline models and their coupling is presented in Figure 2.3. The shelf and shoreline models are connected in two ways: allowing the shelf to influence the nearshore bed levels and using wave parameters calculated by the shelf model to force the shoreline model (Figure 2.3).

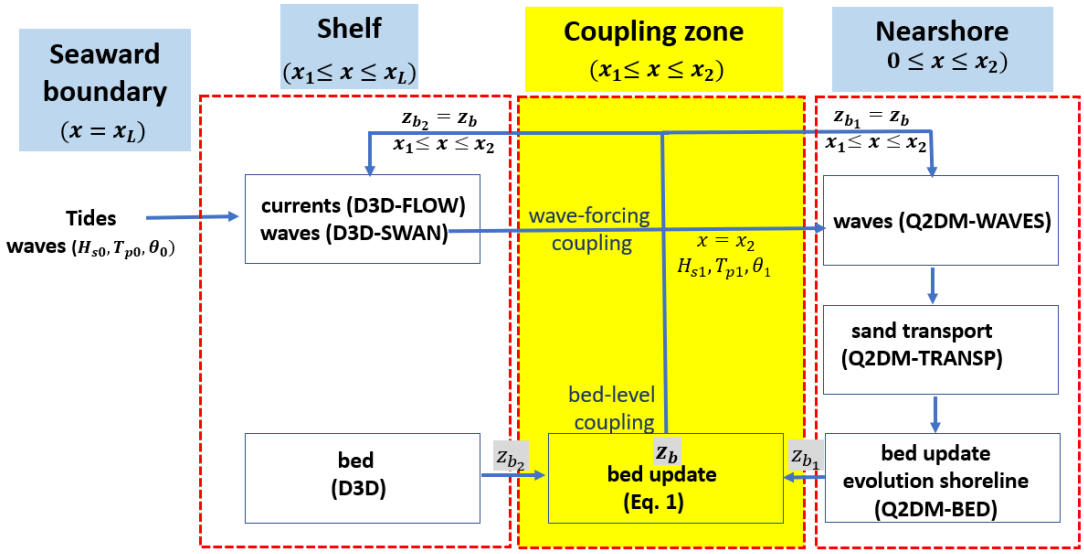

Figure 2.3: The figure depicts a schematic view of the structure of the coupled shelf-shoreline model. The shelf model denoted as D3D (Delft3D), comprises two modules: FLOW and SWAN. These modules compute currents and waves and are forced by tides and waves at seaward boundaries. The shoreline model denoted as Q2DM (Q2Dmorfo), comprises three modules: WAVES, TRANSP, and BED. These modules solve waves, sand transport, and bed-level and shoreline evolution and are forced by waves at $x = x_2$. The coupling between the two models is established by (1) allowing the bed level of the shelf in the coupling zone ($x_1 \leq x \leq x_2$) to affect the bed level of the nearshore (bed-level coupling) and (2) forcing the shoreline model with wave parameters computed by the shelf model (wave-forcing coupling). Further details regarding the model components and coupling are provided in the text. Adapted from Nnafie et al. (2021)

The two models are run separately over time intervals $[t_{n-1}, t_n]$. At each time $t = t_n$, the bed levels of the shoreline and shelf models (z_{b1} and z_{b2}) are used to construct a new bed level (z_b) (Figure 2.2). The bed-level coupling is achieved by combining the seaward portion of the nearshore with the landward portion of the shelf, forming an overlapping area known as the coupling zone. The bed level in this zone, denoted as z_b, is calculated as a weighted average of the bed levels of the shelf (z_{b2}) and nearshore (z_{b1}), with the weighting determined by the function $g(x)$ and a decay width of w, centered at x_0 in the coupling zone, as in Equation 2.18:

$$z_b = g(x)z_{b1} + [1 - g(x)]z_{b2},$$
$$g(x) = \frac{1}{2}\left[1 + \tanh\left(\frac{x - x_0}{w}\right)\right]. \tag{2.18}$$

The bed levels z_{b1} and z_{b2} in the coupling zone are then replaced with z_b, and the wave forcing in the shoreline model is updated with the new wave parameters (H_{s1}, T_{p1}, θ_1) computed by the shelf model (D3D-SWAN) at $x = x_2$. These steps are repeated at each time t_n, with the wave forcing in the shoreline model remaining constant until the next update at t_{n+1}. This process requires frequent data exchange between the different model components, which can be time-consuming.

2.3 Experiments

2.3.1 Prototype System

The Belgium coast, located at the southern edge of the North Sea basin between France and the Netherlands, is selected as a prototype for the shelf-shoreline system. This coast stretches for about 65 km from De Panne in the southwest to Knokke-Heist in the northeast and has a present-day shoreline that is relatively straight and oriented about 40° clockwise from the north. The nearshore region typically has dry beach areas that can be up to 500 m wide at low tide, but there are some locations with little or no dry beach due to shoreline retreat. Offshore on the continental shelf, tidal sand ridges can be found. The Belgium coast is affected by a semi-diurnal tidal wave with a range of 3.6 meters and currents of approximately 0.75 meters per second. Analysis of wave data from 2003 to 2015 shows that waves in the region are predominantly from the south-west and north-west, with mean significant wave heights of around 1 meter, peak periods of approximately 5.7 seconds, and directions with respect to shore normal of approximately 50 degrees for the south-west waves and 0.9 meters, 6.7 seconds, and -32 degrees for the north-west waves (Figure 2.4).

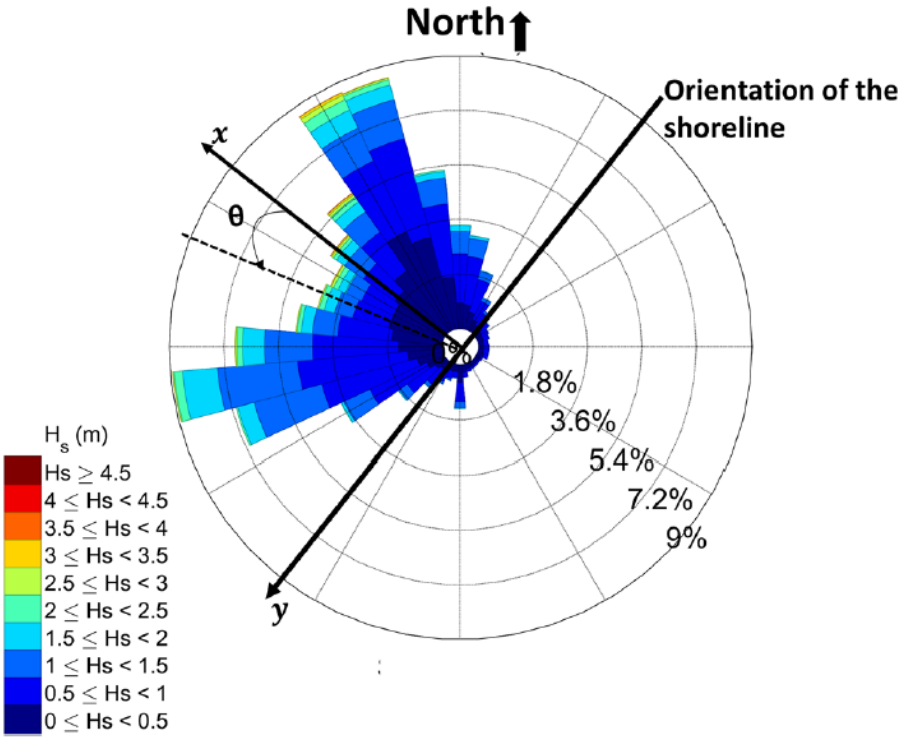

Figure 2.4: The study area's wave rose depicts the relationship between significant wave height (Hs) measured in meters and wave direction (θ) measured in degrees relative to the negative x-axis in a positive anti-clockwise direction. The shoreline is oriented approximately 40° relative to the geographic North. The data used in this study were collected by Rijkswaterstaat, the Ministry of Infrastructure and the Environment in the Netherlands, from wave buoy Deurloo over a period spanning from 2003 to 2015. Adopted from Nnafie et al. (2021)

The shoreface-connected sand ridges at the Belgian shore are about 20 km long, spaced 10-20 km apart, almost shore parallel, and located very close to the coast (Figure 1.7). Their height is 6 meters, about 5 km wide, and they show a rather sharp jump from crest to trough. Notable features concerning the coast are the broad dune areas near the toe of the ridge and shoreline undulations at the point where the shoreface-connected ridge attaches(Verwaest et al., 2020).

2.3.2 Model Configuration and Parameter Setting

In the shelf model, the equations were solved on a rectilinear staggered grid with grid sizes of 750 m and a hydrodynamic time step of 1 minute. These values were chosen based on the study by Nnafie et al. (2020) and were determined to provide accurate results while limiting computation time.

In the shoreline model, the numerical parameters were adopted from Arriaga et al. (2017). The grid size in the alongshore direction was the same as in the shelf model (750 m), but a smaller grid size of 20 m was used in the cross-shore direction to prevent waves from exiting the grid cells through the lateral boundaries and to resolve cross-shore processes in the surf zone adequately. It should be noted that the model was not designed to resolve small-scale processes in the surf zone, such as rip currents. The morphodynamic time step was set to 0.01 days. The shoreline was able to retreat a maximum distance of x_{s0}, the initial width of the dry beach. If the shoreline retreated further, x_s became negative, which the current model version could not handle, causing it to stop.

To mimic the Belgian shelf-shoreline system, the coupled model domain was given dimensions of 55 km by 75 km. The domain length was chosen to be larger than the actual length of the Belgian coast to eliminate the effects of the lateral boundaries on the model results. A dry beach 500 m wide was included at $x_{s0} = 500$ m, and the asymptotic height of the dry beach and the swash slope were set to 1 m and 0.01, respectively, following Arriaga et al. (2017). The coupling zone was defined between 2.5 km and 5 km, and coefficient α, as well as depths H_1 and H_2, were chosen based on a longshore average of the EMODnet bathymetry to approximate the observed cross-shore depth profile $H(x)$. These values were found to be $\alpha =$ 13.7 m, $H_1 = 10$ m, and $H_2 = 43$ m (Nnafie et al., 2021).

The default experiment with ridges has the following characteristics. Two ridges with oblique orientation (75 degrees with respect to shore normal), ridge height of 6 meters, ridge width of 5 km. The ridge is placed realistically far from the beach, with the shoreward tip at 2.5 km from the shoreline at the shoreface and realistically spaced apart (center to center $\sim$ 20 km). See Figure 2.5 for the bottom topography, including shoreface-connected ridges.

The shore-face connected ridges are added to the initial bottom topography as perturbations with respect to the bottom slope. The perturbations have a certain shape comparable with the undulations of shoreface-connected ridges. The SFCR are assumed to resemble a second-order harmonic in the cross-ridge direction to take the sharp transition from trough to edge in account (Figure 2.5). The ridges are constructed to resemble the shoreface-connected ridges

at the Belgian shore. Therefore, they are $\sim$ 6 m high, $\sim$ 5 km wide, $\sim$ 20 km spaced apart laterally, $\sim$ 20 km long, and slightly curved (Houthuys et al., 2021). The mathematical formulations can be found in the appendix.

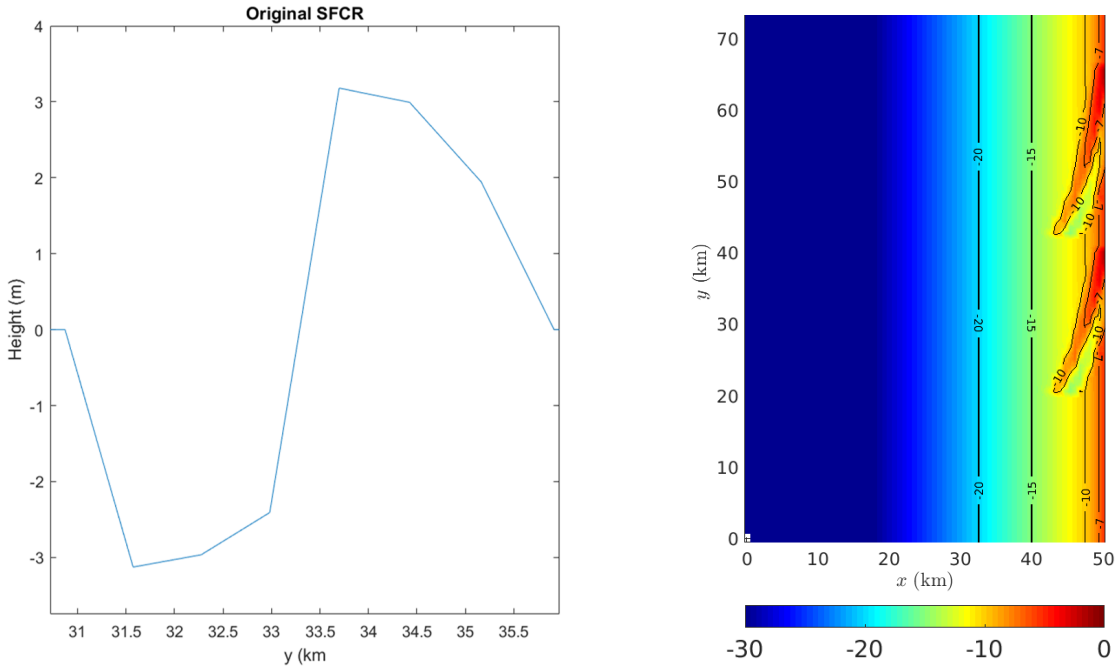

Figure 2.5: a) Cross-ridge profile of constructed artificial ridge. b) Idealized shelf bathymetry in meters below MSL. The ridges are added as perturbations to the background slope.

In the shelf model, time-invariant SW dominant wave conditions were used as a wave forcing at the offshore boundaries. The wave conditions were assumed to have a JONSWAP shape with a peak enhancement factor of 3.3 and directional spreading of 25°. The wave conditions had a significant wave height H_s of 1 m, a peak period T_p of 5.7 s, and a wave direction θ of 50° (south-west, SW) with respect to the shore normal, corresponding to one of two dominant conditions in Figure 2.4. The shelf and nearshore model are coupled with a timestep of 1 year(Nnafie et al., 2021), and the maximum simulation period is 50 years.
Tidal elevation measurements collected at the shelf area of the Belgium coast (available online at http://meetnetvlaamsebanken.be/) were used to prescribe an M2 tidal wave in the shelf model. The tidal wave was set to propagate in the negative y-direction and was imposed along the seaward boundary $x = x_L$, following the procedure suggested by Roelvink and Walstra (2004). The M_2 water-level variations were prescribed with amplitude $\zeta_{M_2} = 1.8$ m and phase difference $\Delta\phi_{M_2} = 31.5°$ between the lateral boundaries $y = 0$, y_L. The seaward boundary is imposed with JONSWAP spectra of incoming waves. These waves are characterized by significant wave height H_{s0}, peak period T_{p0}, and wave direction θ_0, defined relative to the negative x-axis (positive counter-clockwise). Depending on the model experiment, these wave conditions may vary with time. However, it should be noted that the lateral boundaries of the SWAN domain are not periodic, leading to the development of shadow zones with strong reductions in wave height at these boundaries. To avoid any interference of these zones with

model results, the SWAN domain was made larger (75 × 150 km).

The model assumed a sandy seabed comprising of a single sand fraction with a diameter of $d_{50} = 200$ μm, which is representative of the sand grains found in the Belgian coastal zone, as reported by (Deronde et al., 2008). A comprehensive list of all the model parameter values is presented in Table 2.1.

Table 2.1: Model constant input parameters

Parameter	**Value**	**Description**
Model Geometry		
$X_L \times Y_L$	55×75 km^2	Dimensions domain.
x_{s0}	500 m	Initial shoreline position.
$[x_0, x_1, x_2, w]$	$[3950, 2500, 5200, 450]$	Parameters transition zone.
$[b, \beta]$	$\left[1 \text{ m}, 1.9 \times 10^{-3} \text{ m}^{-1}\right]$	Parameters dry beach.
$[A, H_1, H_2]$	$\left[3.55 \times 10^{-3} \text{ m}^{1/3}, 10 \text{ m}, 43 \text{ m}\right]$	Parameters initial depth.
Shelf model		
$[f, C]$	$\left[1.43 \times 10^{-4} \text{ s}^{-1}, 65 \text{ m}^{1/2} \text{ s}^{-1}\right]$	Coriolis and Chezy coefficients.
$[\nu, \epsilon_H]$	$\left[1 \text{ m}^2 \text{ s}^{-1}, 1 \text{ m}^2 \text{ s}^{-1}\right]$	Viscosity and diffusivity coefficients.
$[\alpha_{BS}, \alpha_{BN}]$	$[1, 20]$	Longitudinal and transverse bed slope coefficie
$[\zeta_{M2}, \Delta\psi_{M2}]$	$[1.8 \text{ m}, 31.5°]$	M_2 Tidal forcing.
σ_{M2}	$1.405 \times 10^{-}4$ s^{-1}	Angular frequency M_2 tide.
$[H_{s0}, T_{p0}, \theta_0]$	$[1 \text{ m}, 6 \text{ s}, 50°]$	Wave Forcing Parameters.
Shoreline model		
γ_b	0.5	Breaker index.
d_{50}	0.2 mm	Grain size.
μ	0.1 m$^{1/2}$ s^{-1}	Coefficient CERC formula.
L_2	20 m	Width swash zone.
D_c	8 m	Depth of closure
$[\nu_b, \alpha, \beta]$	$[0.05, 0.46, 0.02]$	Set of non-dimensional parameters.
Numerics shelf model		
Δt	1 min	Timestep.
$[\Delta x, \Delta y]$	$[750 \text{ m}, 750 \text{ m}]$	Size grid cells.
Numerics nearshore model		
Δt	0.01 day	Timestep.
$[\Delta x, \Delta y]$	$[20 \text{ m}, 750 \text{ m}]$	Size grid cells.
Numerics model coupling		
Δt_c	1 year	Coupling time.

2.3.3 Design of Experiments

To address the research questions, multiple experiments were conducted. The first experiment is constructed to address RQ1, which researches differences in tidal currents, wave patterns, sediment transport, and shoreline evolution between the case that ridges on the shelf are absent, respectively present. This involves a comparison of an experiment with SFCR with an investigation that has similar conditions but no SFCR.

The second series of experiments investigates the influence of the distance of the ridge to the shoreline on shoreline evolution (RQ2). All settings are identical to the first experiment except for the distance of the ridge to the shore. The three cases are: Close (2.5 km from the initial shoreline), Intermediate (3.25 km), and Far (4.75 km).

The third series of experiments address ridge orientation's influence on shoreline development (RQ2). The settings are similar to the settings of the first experiment, except for the orientation of the ridge with respect to the coast. This involves four simulations with constant waves from the SW where the orientation of the ridges of the default case is varied, creating ridges with an angle of 70 (Less shore-parallel), 75 (Default), and 80 (More shore-parallel) degrees concerning shore-normal.

The fourth series of experiments investigates the influence of wave direction on shoreline development in the presence of shoreface-connected ridges (RQ3). The settings of the first experiments are used, but instead of south-western waves, the shelf model is forced by JONSWAP spectra with waves from the north-west (NW), with $H_s = 0.9$ m, $T_p = 6.7$ s, and $\theta = -32^\circ$.
The fifth series of experiments investigates the influence of wave direction variation on shoreline development in the presence of shoreface-connected ridges (RQ3). The settings of the first experiments are used, but instead of south-western waves, a more realistic wave climate was utilized by considering time-varying parameters H_s, T_p, and θ, based on the wave record from a nearby station Deurloo Figure 2.4. To mimic the stochastic nature of a realistic wave climate, all wave events were randomly distributed over the 10-year interval, assuming no correlation between individual wave events. To resemble realistic variation of wave characteristics in a wave climate, the model coupling timestep is reduced to 5 days. The resulting synthetic wave climate was used to force the shelf model in this study. The detailed methodology for creating the synthetic wave climate and its classification can be found in Nnafie et al. (2021). Furthermore, the length of the simulation required a shortening of the total simulation period; instead of 50 years, this was set to 10 years.

Table 2.2: Overview of experiments

Experiment name	**Description**
RQ1	
1 - Default case: Ridges | No ridges	Default case with and without ridges for constant SW waves
RQ2	
2 - Distance	As in 1-Ridges, but ridge offshore distance varies between 2.5-4.75 km: Close (2.5 km)| Intermediate (3.25 km)| Far (4.75 km)
3 - Orientation	As in 1-Ridges, but ridge orientation varies between 70-80 degrees: Less shore-parallel (70°) | Default (75°) | More shore-parallel (80°)
RQ3	
4 - Wave Direction SW | NW	As in 1-Ridges, but using constant NW waves
5 - Wave Climate 1 | 2	As in Run1-Ridges, but using two different synthetic wave climates

2.4 Analysis of Model Output

The hydrodynamic conditions on the shelf will be evaluated only at the beginning of the simulation period, as the conditions on the shelf do not change over the simulation period of 50 years. These hydrodynamic conditions determine the wave conditions in the nearshore zone, which are influenced by changes in local bathymetry. The magnitude of the shoreline undulations is evaluated by examining the excursion from the mean, in $x_s'(y,t) = x_s(y,t) - \overline{x_s}(t)$, where $\overline{x_s}(t)$ denotes the average shoreline position at time t. The cross-shore amplitude of shoreline undulations x_s' is expressed by the standard deviation $\sigma_{x_s'}$ of these undulations. This will be used to quantify the temporal evolution of the shoreline undulations. This is accompanied by the evolution of the mean position of the shoreline $\bar{x's}(t)$ in time. Changes in sand volume in the nearshore shoreline area are calculated by

$$\Delta V = \int_{y_0}^{y_L} \int_{x0}^{x=2\text{ km}} (z_b(x,y,t) - z_b(x,y,t=0))dxdy. \tag{2.19}$$

For experiments with different ridge orientations and distances concerning the coast, the difference between the respective shoreline positions of cases 1 and 2 are calculated by

$$\Delta \int_{y=0}^{y=y_L} x_s dy = \int_{y=0}^{y=y_L} x_{s,1} dy - \int_{y=0}^{y=y_L} x_{s,2} dy. \tag{2.20}$$

To avoid boundary effects, the analysis of model results focuses on the region $5 \leq y \leq 70$ km.

3 | Results

3.1 Effect of shoreface-connected ridges on hydrodynamics, sediment transport, and shoreline evolution

The presence of shoreface-connected ridges affects the hydrodynamics on the shelf. A northward propagating M2-tidal wave is prescribed at the offshore boundary. As shown in Figure 3.1, the tidal amplitude increases from the western boundary to the eastern boundary from 1.8 m to 2.3 m in the zones where ridges are absent. When ridges are present, they locally increase the tidal amplitude to 2.5 m.

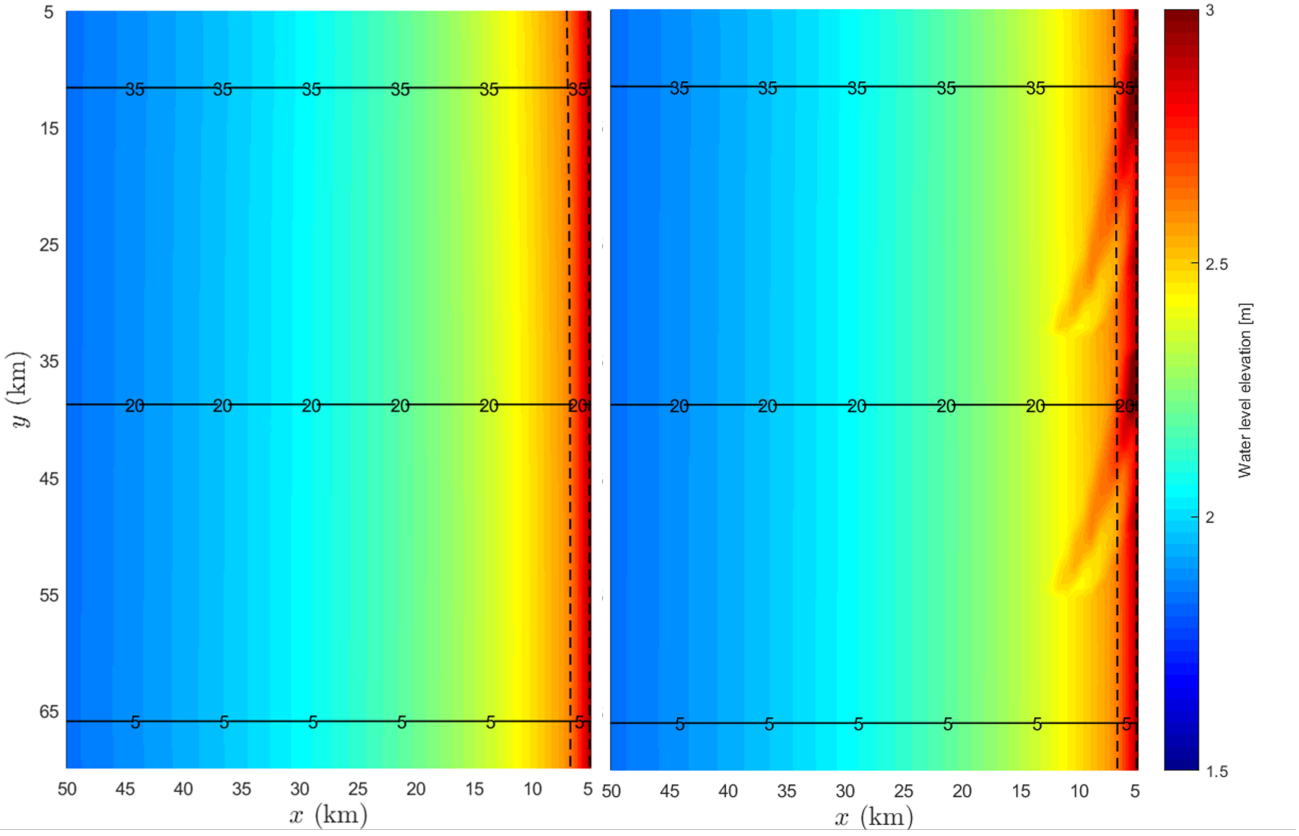

Figure 3.1: Spatial distribution of amplitude (colors) and phase (solid lines) of tidal sea surface height on the shelf in the absence of ridges. b) As a), but with ridges present.

Furthermore, the presence of the ridges significantly impacts the tidal current magnitude and direction. In Figure 3.2 the currents during flood conditions ($\eta > 0$) are shown. The currents on the ridges are weaker compared to when ridges are not present there ($\Delta U \sim 0.15$ m/s). Furthermore, the currents are directed more onshore in the troughs of the ridges and more offshore on the crests of the ridges. The currents' direction gets increasingly shoreward from the eastern boundary towards the western boundary. The average M_2 current velocity magnitude ranges between 0.5 m/s and 0.8 m/s, comparable to previously reported values (Bindels, 2020, and references therein).

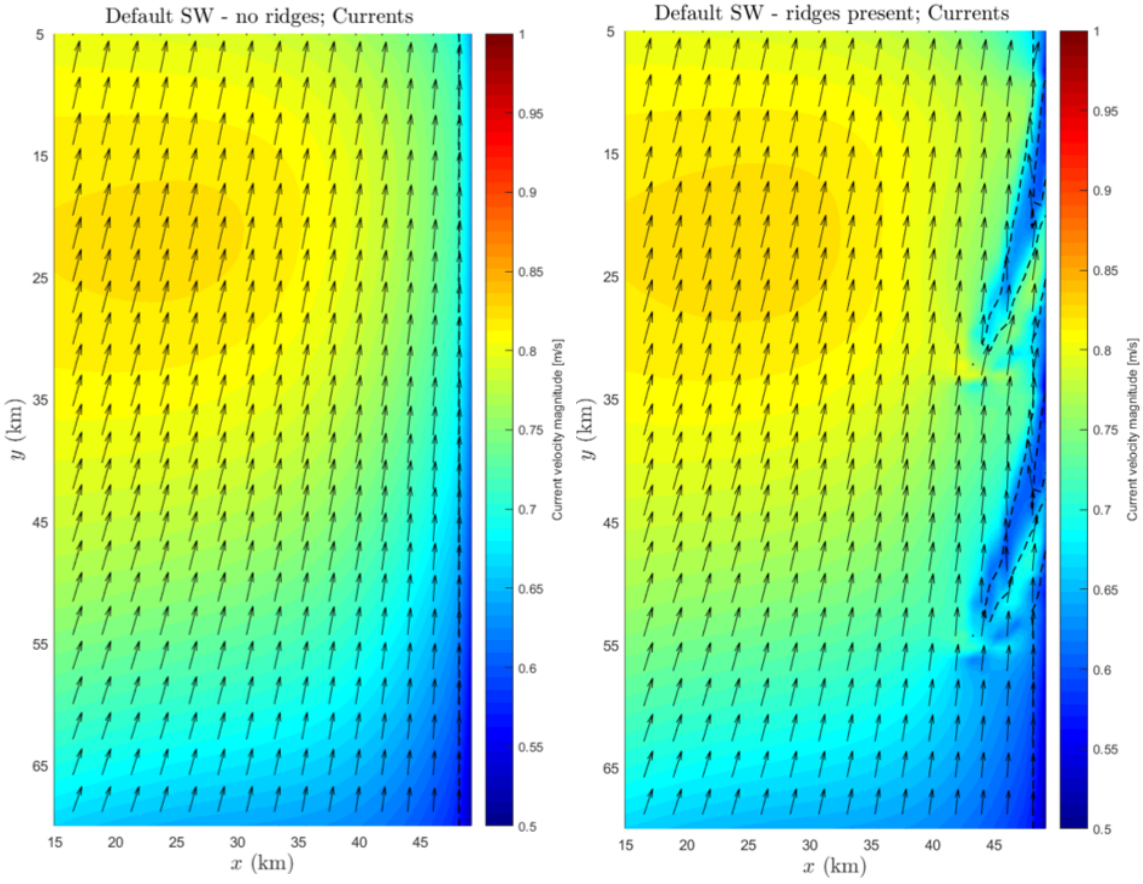

(a) **(b)**

Figure 3.2: a) Current velocities on the shelf during high water ($\phi = 0°$) at the southern boundary ($y = y_L$) when ridges are absent. Colors indicate current velocity magnitude; arrows indicate the flow direction, and bathymetry contours are in dotted black lines. b) As a), but with ridges present.

Waves

Waves on the shelf are significantly influenced by the presence of shoreface-connected ridges. This is shown in Figure 3.3. On the offshore boundary JONSWAP spectra with $H_{s0} = 1$ m, $T_{p0} = 6$ s and $\theta_0 = 45°$ are forced. Due to propagation over the shelf, the waves are refracting, changing direction towards 35° on the nearshore (eastern) boundary of the shelf. In the presence of ridges, this effect varies locally. On the crests of the ridges, waves are refracted more, decreasing the angle with the shore-normal further ($\sim 25°$), whereas the opposite occurs in the troughs leading to more shore-parallel waves ($\sim 45°$).

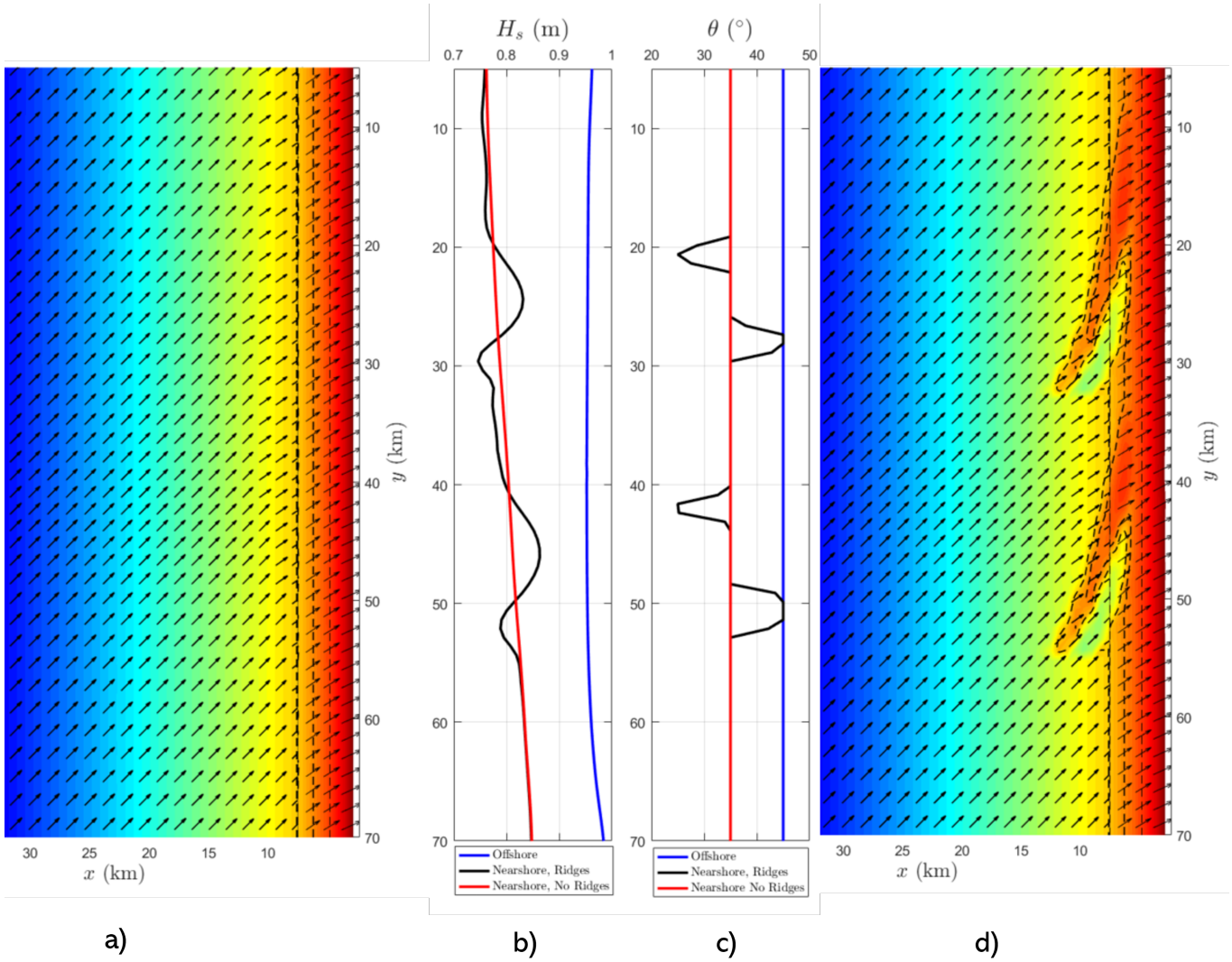

Figure 3.3: a) Wave vector (arrows) plotted on the default bathymetry (color) when forced with constant SW waves at the boundary when ridges are absent. b) The significant wave height H_s versus longshore distance y at the offshore boundary ($x = 50$ km, blue line) and the nearshore boundary ($x = 5$ km, red and black lines for the case without and with ridges, respectively). b) As a), but with ridges present.

The significant wave height is also affected by the presence of ridges. Due to propagation over the shelf, the significant wave height decreases between the offshore boundary at $x = 50$ km ($H_s \sim 0.95$ m) and the boundary with the nearshore zone at $x = 5$ km ($H_s \sim 0.8$ m). The significant wave height increases alongshore in the positive y-direction. Again, the presence of ridges leads to local variation in significant wave height. This is due to increased shoaling over the ridge crest, where propagation over the shallower bed increases significant wave height compared to the deeper trough.

Sediment transport

The hydrodynamic template results in spatial variation in sediment transport. In Figure 3.4 cross-shore integrated (from the shoreline x_s to the depth of closure $D_c = 8$ m) longshore and cross-shore sediment transport rates (respectively Q_y and Q_x) are shown in combination with a zoom in of the sediment transport rates in the nearshore zone near the southern ridge, between $y = 30$ km and $y = 50$ km. The magnitude of the longshore sediment transport rate ($Q_y \sim 5 \cdot 10^5$ m^3/year) is similar for the cases with and without ridges and is larger than the cross-shore sediment transport rate ($Q_x \sim 0.1 \cdot 10^5$ m^3/year). If no ridges are present, the alongshore sediment transport rate is uniform in the longshore direction. When ridges are present, however, significant gradients in longshore sediment transport occur, which correspond to the locations of the wave-energy hotspots between $y = 30$ km and $y = 50$ km. Interestingly, this area corresponds to the zones where significant cross-shore sediment transport is identified. A closer look at the spatial distribution of the sediment transport shows that the cross-shore sediment transport towards the coast ($Q_x < 0$) is found in the area between $y = 36$ km and $y = 46$ km, and from $x = 3$ km to $x = 5$ km. This zone is absent when ridges are absent and corresponds to the location of the shoreward end of the ridge.

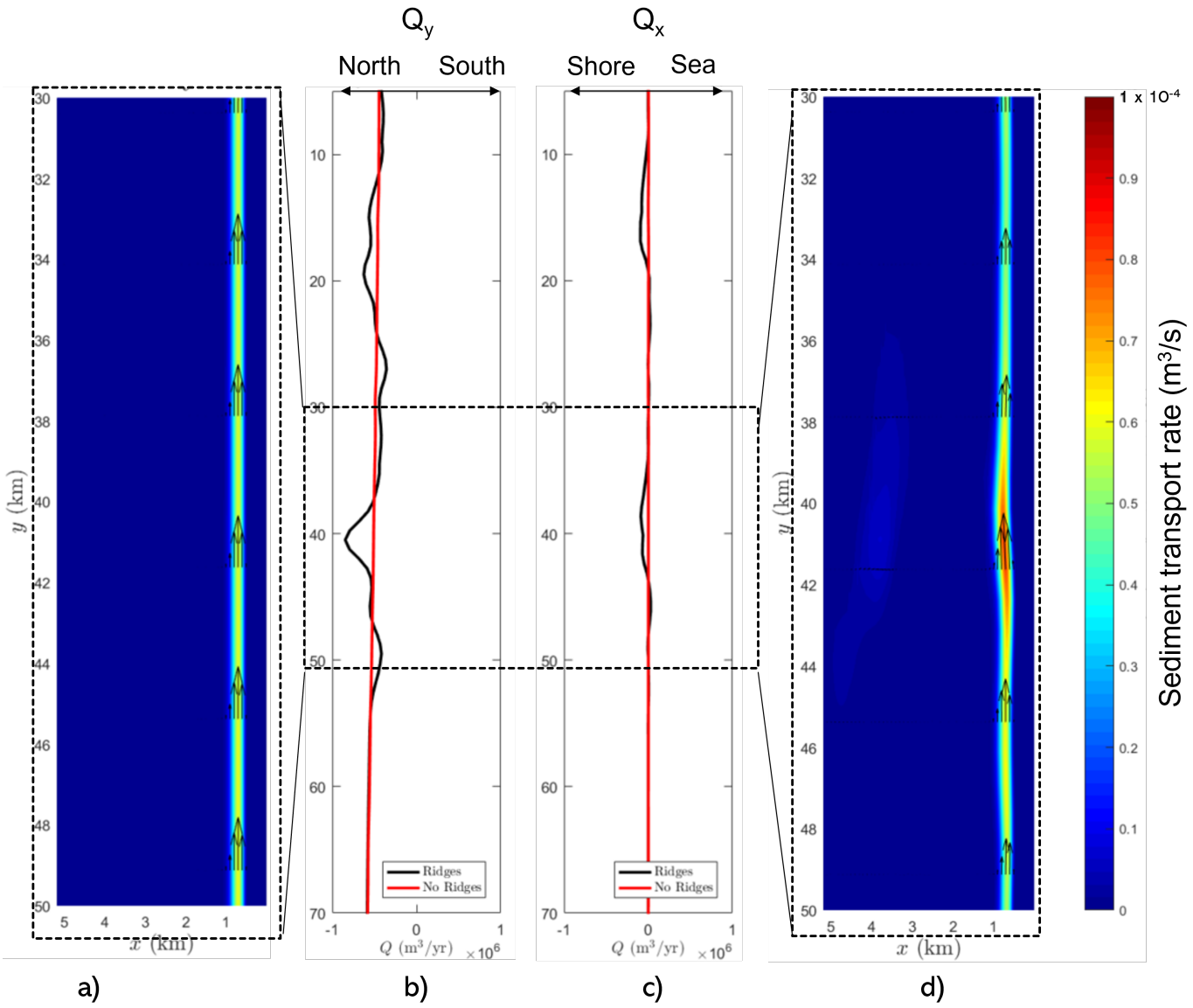

Figure 3.4: a) Color plot of the spatial distribution of total sediment transport rate at $t = 1$ year in the nearshore zone between $y = 30$ km and $y = 50$ km when ridges are absent. The black arrows are the total sediment transport vectors. b) The cross-shore integrated (from the shoreline x_s to the depth of closure $D_c = 8$ m) longshore component of the total sediment transport when ridges are absent (red line), and ridges are present (black line). Negative (positive) values indicate transport to the north (south). c) The cross-shore integrated (from the shoreline x_s to the depth of closure $D_c = 8$ m) cross-shore component of the total sediment transport when ridges are absent (red line), and ridges are present (black line). Negative (positive) values indicate transport to the shore (sea). d) As a), but with ridges present.

Shoreline evolution

The combination of the gradients in littoral drift and onshore-directed cross-shore transport lead to changes in the morphology of the nearshore zone. Figure 3.5 shows the bathymetry and shoreline position after 15 years. This moment is chosen as instabilities start occurring shortly hereafter. Small undulations ($\sigma_{x_s'} \sim 20$ m) are found in the absence of ridges. These undulations do not maintain their relative position but travel alongshore northward. At $t = 15$ years, they are found at $y \approx 52$ km and $y \approx 35$ km, see Figure 3.12, and resemble shoreline sand waves.

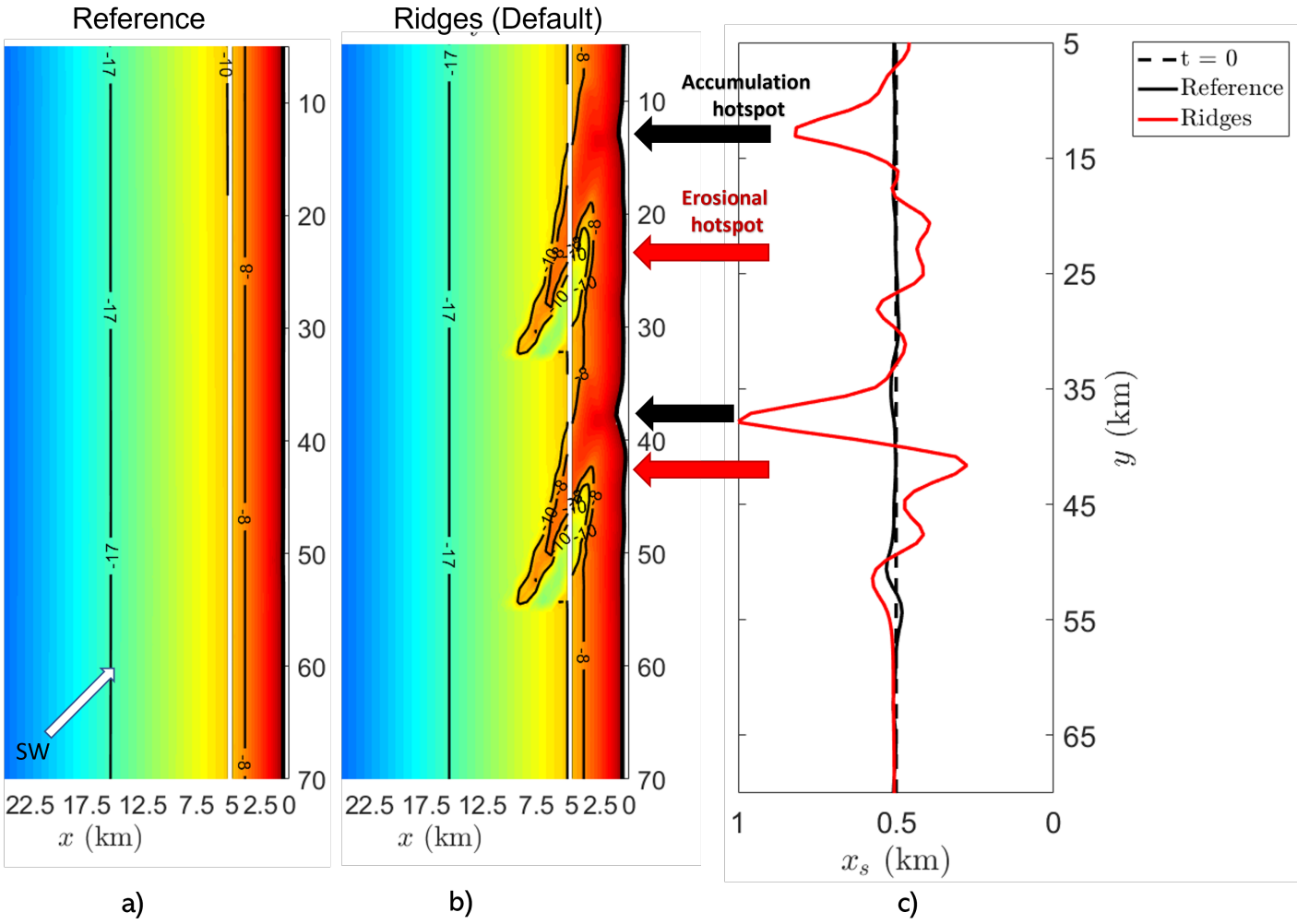

Figure 3.5: a) Color plot of the bathymetry of the shelf and nearshore after 15 years. The shoreline position, x_s, is denoted by the thick black line that separates the dry beach (white area) from the submerged bed (colored). b) As a), but when ridges are present. c) Shoreline positions x_s plotted againts longshore position (y) at $t = 15$ years. The dotted line represents the initial shoreline position at $t = 0$; the black line represents the case where ridges are absent (Reference), and the red line represents the case where ridges are present (Default). The position of accumulation hotspots (erosional hotspots) is denoted by the large black (red) arrows.

When ridges are present, two main developments stand out. First, large shoreline undulations with a longshore extend of $\sim$ 25 km and maximum cross-shore amplitude of $\sim$ 0.2 km have formed. The accumulation hotspots ($x_s > x_{s0}$) coincide with the position of the crest of the shoreface-connected ridges and the position of the largest gradient in littoral drift $\partial Q_y/\partial y > 0$, and the position of the largest shoreward sediment flux $Q_x < 0$. The erosion hotspots ($x_s < x_{s0}$) are located up-drift (negative y-direction) of the accretion hotspots and coincide with the position of the trough of the shoreface-connected ridges, the position of the largest gradient in littoral drift $\partial Q_y/\partial y < 0$, and the position of the largest seaward sediment flux $Q_x > 0$. Note that the seaward extend of the accumulation zone ($x's \sim 500$ m) is larger than the shoreward retreat in the erosion zone ($x's \sim 200$ m). Furthermore, the accumulation and erosional hotspots near the northern ridge at $y = 15$ km are smaller in magnitude (respectively $x's \sim 250$ m and $x's \sim 100$ m) than the undulations near the southern ridge at $y = 45$ km, but have the same longshore extend ($\sim$ 25 km, similar to the ridges). This is due to the decrease of wave energy towards the north, leading to lower rates of littoral drift and, therefore, smaller absolute gradients of littoral drift, while cross-shore sediment fluxes are comparable.

3.2 The influence of ridge characteristics on decadal shoreline evolution

3.2.1 Sensitivity to distance to the coast

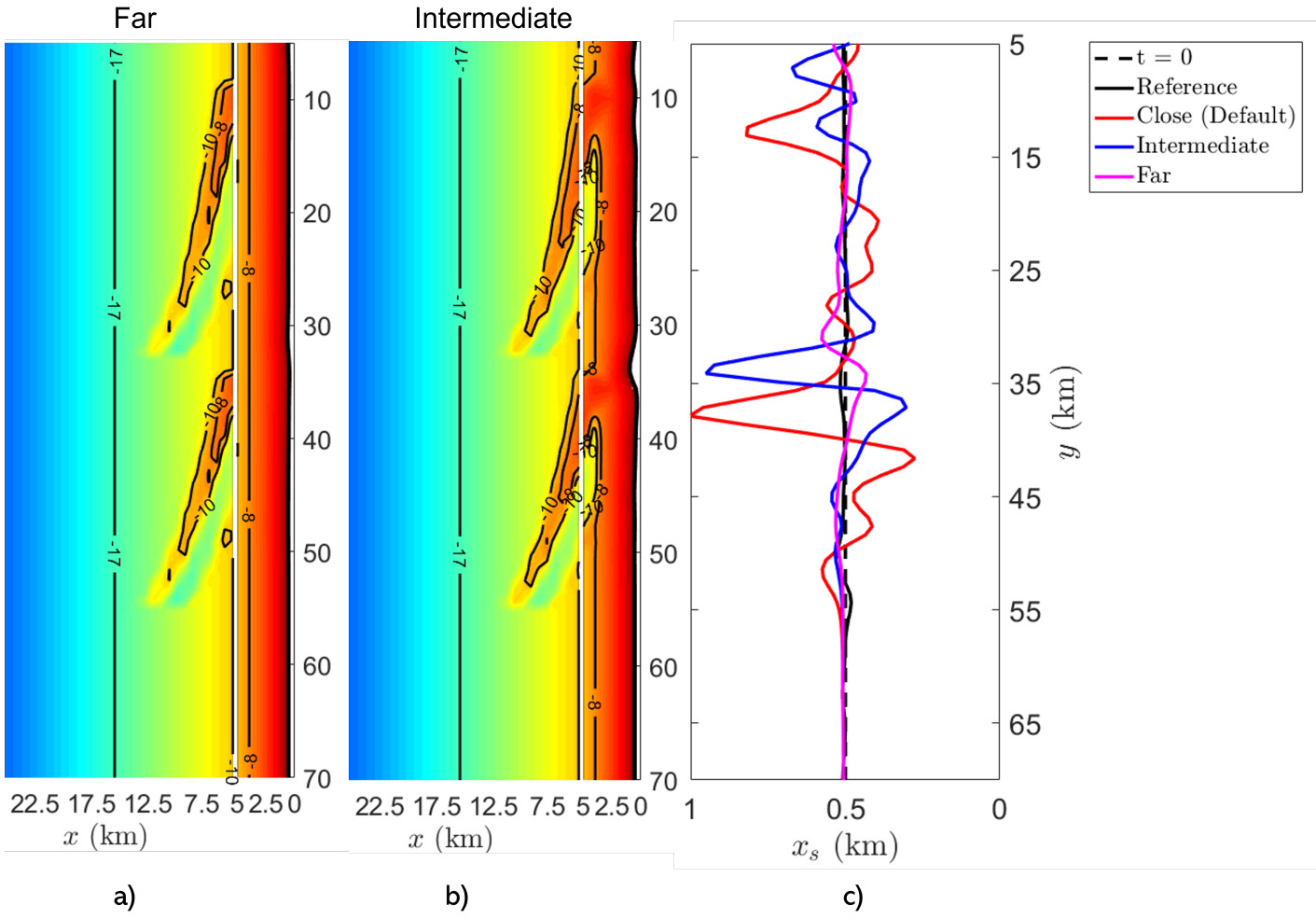

Figure 3.6: a) Color plot of the bathymetry of the shelf and nearshore after 15 years for the case where ridges at 4.75 km from the shore (Far, see RQ2 in Table 2.2). The shoreline position, x_s, is denoted by the thick black line that separates the dry beach (white area) from the submerged bed (colored). b) As a), but when ridges are present at 3.25 km from the shore (Intermediate, see RQ2 in Table 2.2). c) Shoreline positions x_s plotted against longshore position (y) at t = 15 years, for the initial position (dotted black line), reference case (black line), ridges are close (Default, red line), intermediate (blue line), and far (magenta line).

In Figure 3.6 the results for the distance experiment (see RQ2, experiment 2 in Table 2.2) are shown. The comparison of shoreline position x_s near the southern ridge between the cases at $t = 15$ years shows that the magnitude of the accumulation (erosion) hotspot for ridges close to the shoreline (2.5 km, Default case) is largest with $x_s' = +500$ m ($x_s' = -200$ m), compared to the Intermediate case with $x_s' \approx +400$ m ($x_s' \approx -175$ m), and Far case $x_s' \approx +50$ m ($x_s' \approx -50$ m). The same trend is visible at the northern ridge for smaller magnitudes. The position of the accumulation (erosion) hotspot near the southern ridge is at $y = 38$ km ($y = 45$ km) for the Close case, $y = 34$ km ($y = 40$ km) for the Intermediate case, and $y = 31$ km ($y = 35$ km) for the Far case, shifting north with ridge distance to the shoreline.

In the first ten years, the development of shoreline undulations amplitude $\sigma_{x_s'}$ is fastest for ridges at 3.25 km (intermediate) distance (Figure 3.7a). After t = 10 years, the section of exponential growth of the shoreline undulations starts in the case of the ridges at 2.5 km, while the shoreline undulations and mean shoreline keep growing steadily for the two cases with ridges further offshore. The exponential growth for the case of 2.5 km distance from the coast (Close) is attributed to the increase in shoreward cross-shore sediment flux (Q_x). This effect is weaker for the case of the ridges at 3.25 km distance (Intermediate), where this occurs after t = 20 years, and absent for ridges at 4.75 km distance (Far). This translates to an increase in shoreline sediment volume as visible in Figure 3.7b). For close ridges, this leads to an increase in shoreline volume per square meter of $\sim$ 70 mm after 15 years, an increase in which shoreline in the presence of the far ridges reaches after 50 years. For ridges at the intermediate position, increase in shoreline volume per square meter of $\sim$ 30 mm after 20 years. When no ridges are present, the shoreline volume increased with $\sim$ 20 mm after 50 years.

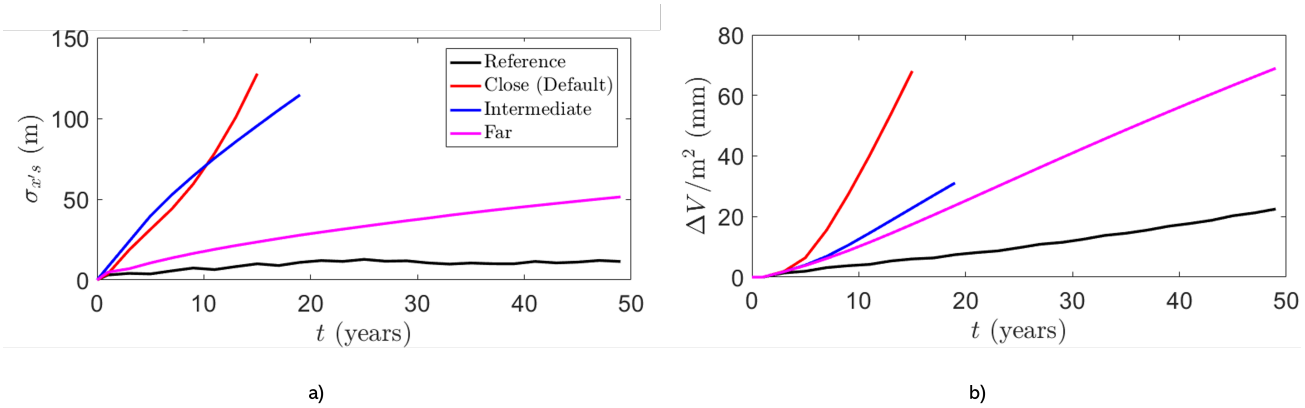

Figure 3.7: a) Shoreline undulation amplitude $\sigma_{x_s'}$ plotted against time, for the reference case (black line), ridges are close (Default, red line), intermediate (blue line), and far (magenta line). b) As a), but now volume change per m^2 (mm) compared to initial conditions in the upper nearshore zone (between $x = 0$ and $x = 2.5$ km) is plotted against time.

The difference in the integrated shoreline position ($\frac{1}{L}\Delta \int x_s dy$) and increased shoreline volume ($\Delta V/\mathrm{m}^2$) between the Far, Intermediate, and Close cases are used to evaluate the effect of onshore propagation of ridges. In Figure 3.8, this is plotted. When the far ridges are moved to the intermediate position, a slight seaward shift of the integrated shoreline position in the

order of 1 m is observed after 15 years, resulting in relative growth of the shoreline volume of 5 mm per m^2. This effect is much more significant when ridges are moved from the intermediate to the close position. The mean integrated shoreline position shifts $\sim$ 20 m seaward. This leads to a relative increase in shoreline volume of 40 mm per m^2 for ridges positioned 750 m more onshore over 15 years. This is in the same order of magnitude as current rates of sea level rise (3.3 mm/year (Pickering et al., 2012)), which translates to an increase in mean sea level by 50 mm over 15 years. Furthermore, these ridges are not instantaneously transferred between the positions. Following Houthuys et al. (2021), the ridges at the Belgian shore are migrating onshore at a rate of 3 - 20 m/year, taking 250 - 40 years to move 750 m onshore. This implies that the actual change in shoreline volume due to the onshore movement of ridges is smaller than the difference plotted in Figure 3.8b. Therefore, the results suggest that current sea-level rise rates will likely overshadow the increase in shoreline position.

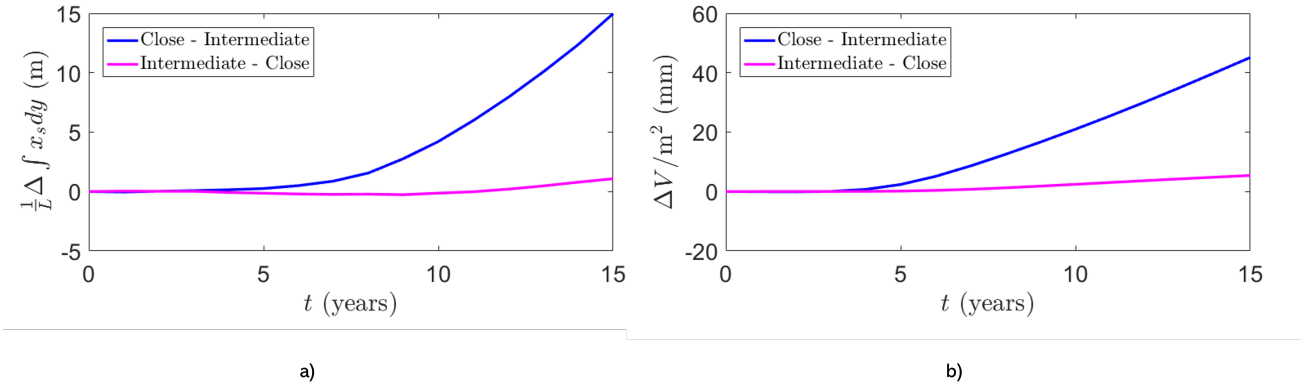

Figure 3.8: a) Difference in integrated shoreline position per meter (longshore) between close ridges and intermediate ridges (blue line) and intermediate ridges and far ridges (magenta line), plotted against time. b) As a), but now for, the difference in volume change per m^2 (mm) in the upper nearshore zone (between $x = 0$ and $x = 2.5$ km) is plotted against time.

In short, the accumulation and erosional hotspots shift towards the north with increasing distance of sfcr to the shoreline. The more onshore the ridges, the stronger the undulations. Onshore movement of the ridges results in an increase in shoreline volume. This effect is stronger for more onshore ridges but remains smaller than the increase of MSL due to sea level rise.

3.2.2 Sensitivity to ridge orientation

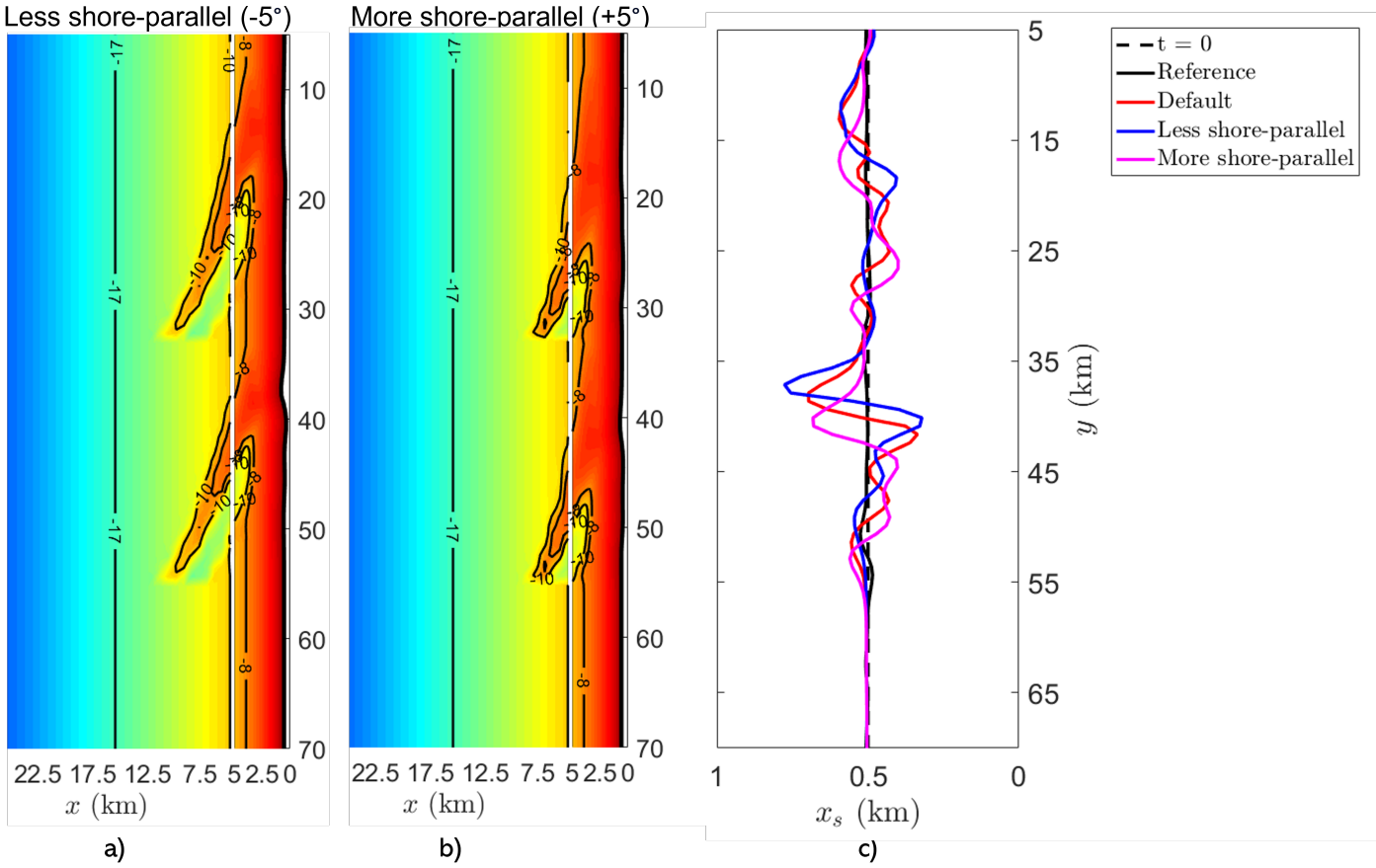

Figure 3.9: a) Color plot of the bathymetry of the shelf and nearshore after ten years for the case where ridges are oriented less shore-parallel (-5°) compared to the default case (see Experiment 3 in Table 2.2). The shoreline position, x_s, is denoted by the thick black line that separates the dry beach (white area) from the submerged bed (colored). b) As a), but when ridges are oriented more shore-parallel (+5°) compared to the default case. c) Shoreline positions x_s plotted against longshore position (y) at t = 15 years, for the initial position (dotted black line), reference case (black line), default ridges (red line), less shore-parallel (blue line), and more shore-parallel (magenta line).

In Figure 3.9 the results for the orientation experiment (see RQ2, experiment 3 in Table 2.2) are shown at $t = 10$ years, as shortly hereafter the less-shore parallel simulation started showing instabilities. The comparison of shoreline position x_s near the southern ridge between the cases at $t = 10$ years shows that the magnitude of the accumulation (erosion) hotspot for ridges oriented less shore-parallel is largest with $x_s' \approx +275$ m ($x_s' \approx -200$ m) compared to the default ridges with $x_s' \approx +200$ m ($x_s' \approx -190$ m), and ridges oriented more shore-parallel $x_s' \approx +190$ m ($x_s' \approx -50$ m). At the northern ridge, magnitudes are similar, with accumulation (erosion) hotspots of $x_s' \approx +100$ m ($x_s' \approx -50$ m). The position of the accumulation (erosion) hotspot near the southern ridge is at $y = 36$ km ($y = 42$ km) for the less shore-parallel ridges, $y = 38$ km ($y = 44$ km) for the default ridges, and $y = 40$ km ($y = 47$ km) for the Far case,

shifting south with ridge orientation more parallel to the shoreline.

After t = 13 years, instabilities arise in the case of the less shore-parallel ridges, while the shoreline undulations and mean shoreline keep growing steadily for the two cases with default ridges and more shore-parallel ridges. In the first 12 years, the development of shoreline undulations amplitude $\sigma_{x'_s}$ in the presence of more shore-parallel ridges is similar to default ridges and fastest in the presence of less shore-parallel ridges (Figure 3.10a). The exponential growth for the case of less shore-parallel ridges is attributed to the increase in shoreline curvature, exceeding the limits to which the numerical model is stable. This effect occurs later for the default ridges (after 15 years) and more shore-parallel ridges (after t = 15 years). The sediment volume change in the shoreline area compared to the initial situation is shown in Figure 3.7b). After ten years, the increase of volume is largest for the more shore-parallel ridges $\sim$ 40 mm, compared to the default ridges $\sim$ 30 mm, and the less shore-parallel ridges $\sim$ 20 mm.

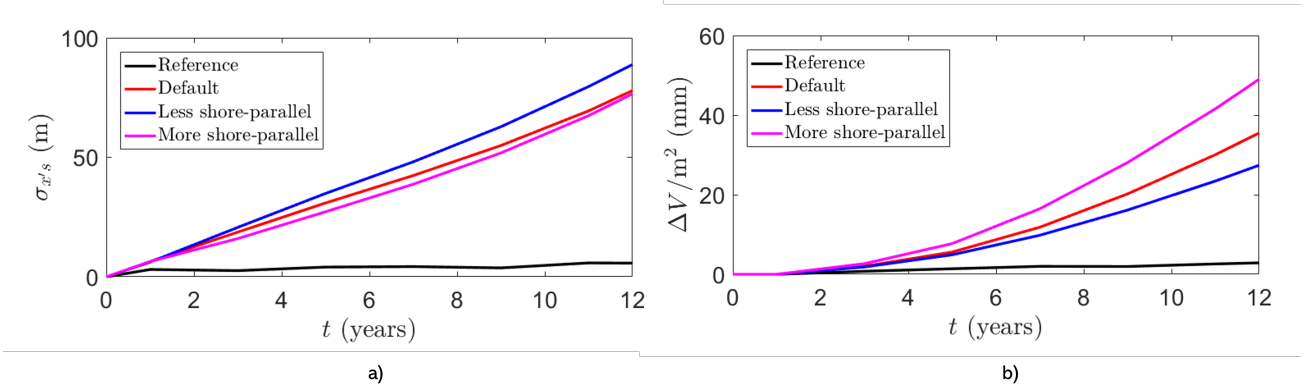

Figure 3.10: a) Shoreline undulation amplitude $\sigma_{x'_s}$ plotted against time for the reference case (black line), default ridges (red line), less shore-parallel (blue line), and more shore-parallel (magenta line). b) As a), but now volume change per m^2 (mm) compared to initial conditions in the upper nearshore zone (between $x = 0$ and $x = 2.5$ km) is plotted against time.

The difference in the shoreline position $\frac{1}{L}\Delta \int x_s dy$ and increase shoreline volume $\Delta V/\mathrm{m}^2$ between the default, less shore-parallel, and more shore-parallel cases are used to evaluate the difference of a ridges change in orientation. In Figure 3.8, this is plotted. When the orientation of the default ridges change to a less shore-parallel orientation, a slight seaward shift of the integrated shoreline position in the order of a 1 m is observed after 12 years, resulting in a relative decrease in shoreline volume of -25 mm per m^2, which is net erosion. When ridges change from the default orientation to a more shore parallel orientation, the mean integrated shoreline position shifts $\sim$ 2 m landward. This leads to a relative increase in shoreline volume of 40 mm per m^2 over 12 years, leading to net accretion.

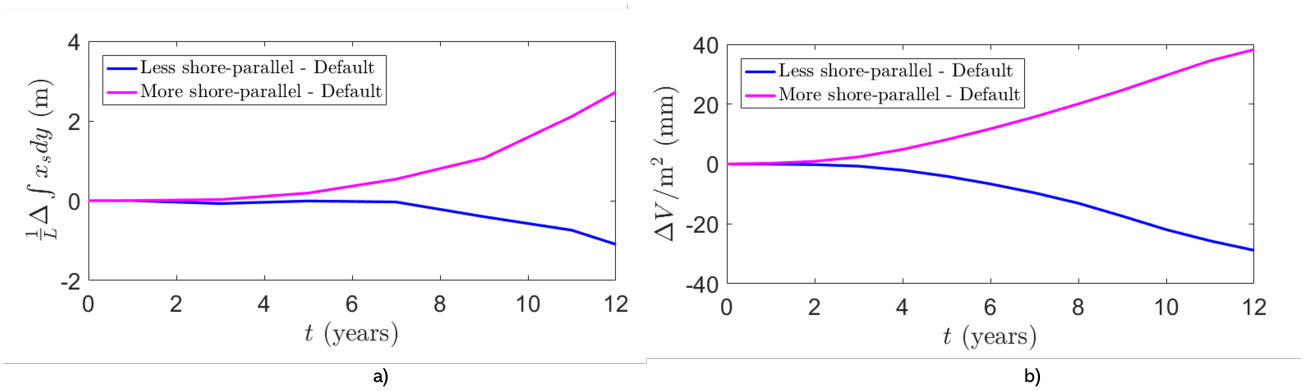

Figure 3.11: a) Difference in integrated shoreline position per meter (longshore) between less shore-parallel ridges and default ridges (blue line) and more shore-parallel ridges and default ridges (magenta line), plotted against time. b) As a), but now for, the difference in volume change per m^2 (mm) in the upper nearshore zone (between $x = 0$ and $x = 2.5$ km) is plotted against time.

The experiment results show that the magnitude of the shoreline undulations is most significant with the less shore-parallel ridges (Angle = 70 degrees) and smallest for the most shore-parallel ridge (Angle = 80 degrees). This conforms to expectations, as the crests of the more shore-normal ridges are better aligned with the southwestern waves. The shape and relative position of the shoreline undulations are comparable. Furthermore, the spatial extent in the longshore direction is similar to the longshore extent of the ridges ($\sim$ 25 km) for all cases. The results show that accumulation and erosional hotspots shift towards the south with more shore-parallel orientation. The strength of the undulations changes due to the ridge's orientation; the more shore-parallel the orientation, the weaker the undulations.

3.3 The influence of wave variation on decadal shoreline evolution

3.3.1 Sensitivity to wave direction

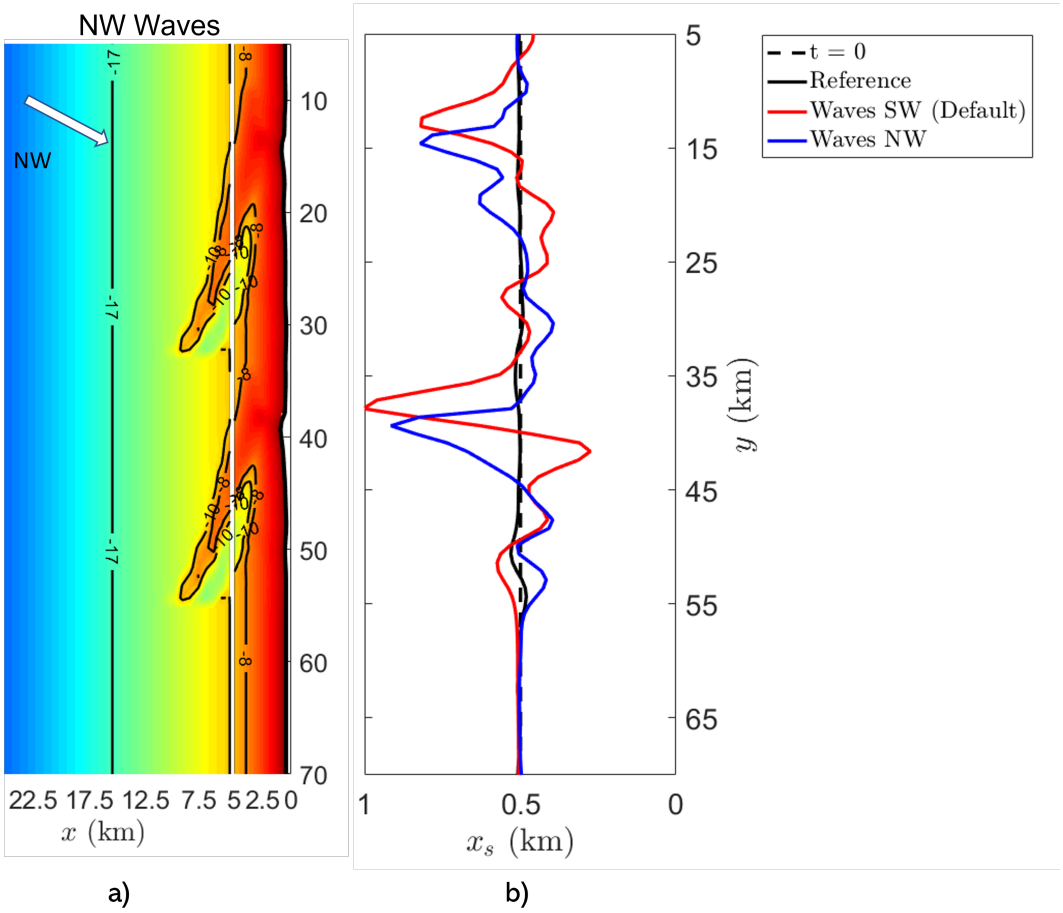

Figure 3.12: a) Color plot of the bathymetry of the shelf and nearshore after 15 years for the case where default ridges are forced by constant waves from the northwest (see Experiment 4 in Table 2.2). The shoreline position, x_s, is denoted by the thick black line that separates the dry beach (white area) from the submerged bed (colored). b) Shoreline positions x_s plotted against longshore position (y) at $t = 15$ years, for the initial position (dotted black line), reference case (black line), default ridges forced waves from the south-west (red line) and default ridges forced waves from the north-west (blue line).

The results of the wave direction experiment are shown in Figure 3.12 for the cases with south-western and north-western waves. The formation of large-scale coastline undulations is observed in both cases. Especially for the case of south-western waves, it is clear that an erosion hotspot occurs on the location of the trough of the southern ridge ($x_s' \approx -200$ m), which is larger than the magnitude of the erosion hotspot for north-western waves ($x_s' \approx -100$ m). Accumulation hotspots are found near the crests of the ridges. They are comparable in size near the northern ridge $x_s' \approx +300$ m, and slightly larger for southwestern waves at the

southern ridge ($x_s' \approx +500$ m) than for north-western waves ($x_s' \approx +450$ m). After 15 years, the position of the coastline undulations is slightly shifted with respect to each other. Accretion and erosion hotspots have shifted towards the south when the direction of incoming waves changes from southwest to northwest, in line with the relative position of ridges compared to the incoming wave direction. The longshore extension of the shoreline undulation is ~ 25 km, similar to the longshore extent of the ridges.
The evolution of the undulations for NW and SW waves is similar, where the amplitude $\sigma_{x_s'}$ of the shoreline undulations for SW waves are slightly larger after 15 years. The volume increase in the case of NW waves is larger than for SW waves over the whole simulation period, and after 15 years, this difference is ~ 20 mm. This difference lies in the smaller eroded area for NW waves.

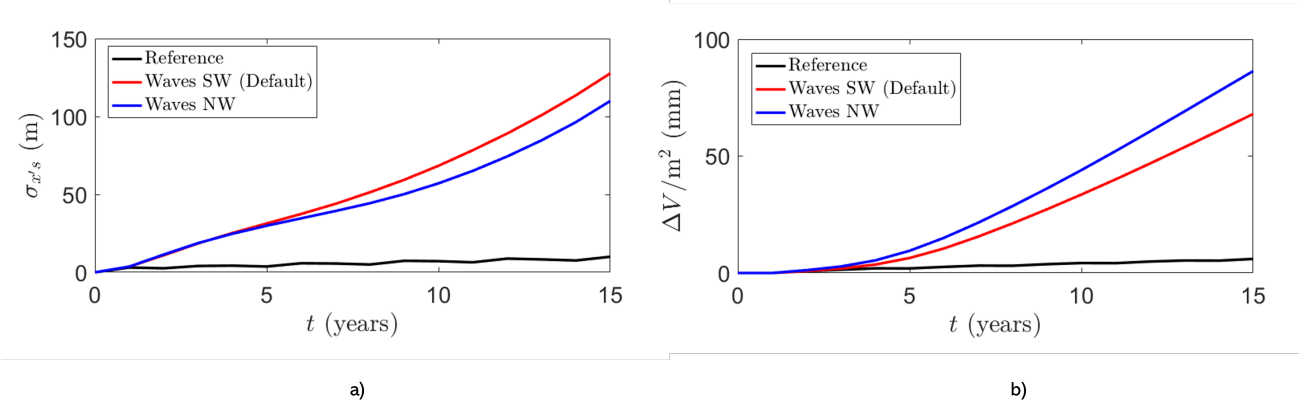

Figure 3.13: a) Shoreline undulation amplitude $\sigma_{x_s'}$ plotted against time, for the reference case (black line), default ridges forced with constant waves from the southwest (red line), and constant waves from the north-west (blue line). b) As a), but now volume change per m^2 (mm) compared to initial conditions in the upper nearshore zone (between $x = 0$ and $x = 2.5$ km) is plotted against time.

3.3.2 Sensitivity to variable wave forcing

In Figure 3.14 the results for experiment Run5 (Table 2.2) are shown. Note that here only ten years are simulated due to the long simulation times involved with a coupling timestep of 5 days. The shoreline profile in the case of the two wave climates differs from the profile of the constant waves from the southwest. After ten years, the magnitude of the cross-shore extend of the shoreline position has reached ~ 2 km for constant SW waves. The shoreline undulations for the two wave climate scenarios extend to a maximum position of 1.5 km, and overall these are about ~ 2.5 times smaller. This large factor is due to the small erosion areas next to the progradation area. The longshore extend of the shoreline undulations are ~ 25 km for both the constant waves from the SW and the two wave climates, similar to the size of the ridges. The relative position of the large protrusion area compared to the ridge is roughly the same. Since the position of the protrusion area is similar for constant NW waves and SW waves, the two dominant wave directions that make up the wave climate (Figure 2.4), this conforms to expectations. Note the surprisingly large undulations already present after ten years of evolution. In the default case with SW waves and a coupling timestep of 1 year,

the maximum cross-shore extent of the shoreline undulation does not reach this cross-shore extent. The location of accumulation and erosional hotspots are not influenced, but the wave variation weakens the undulations.

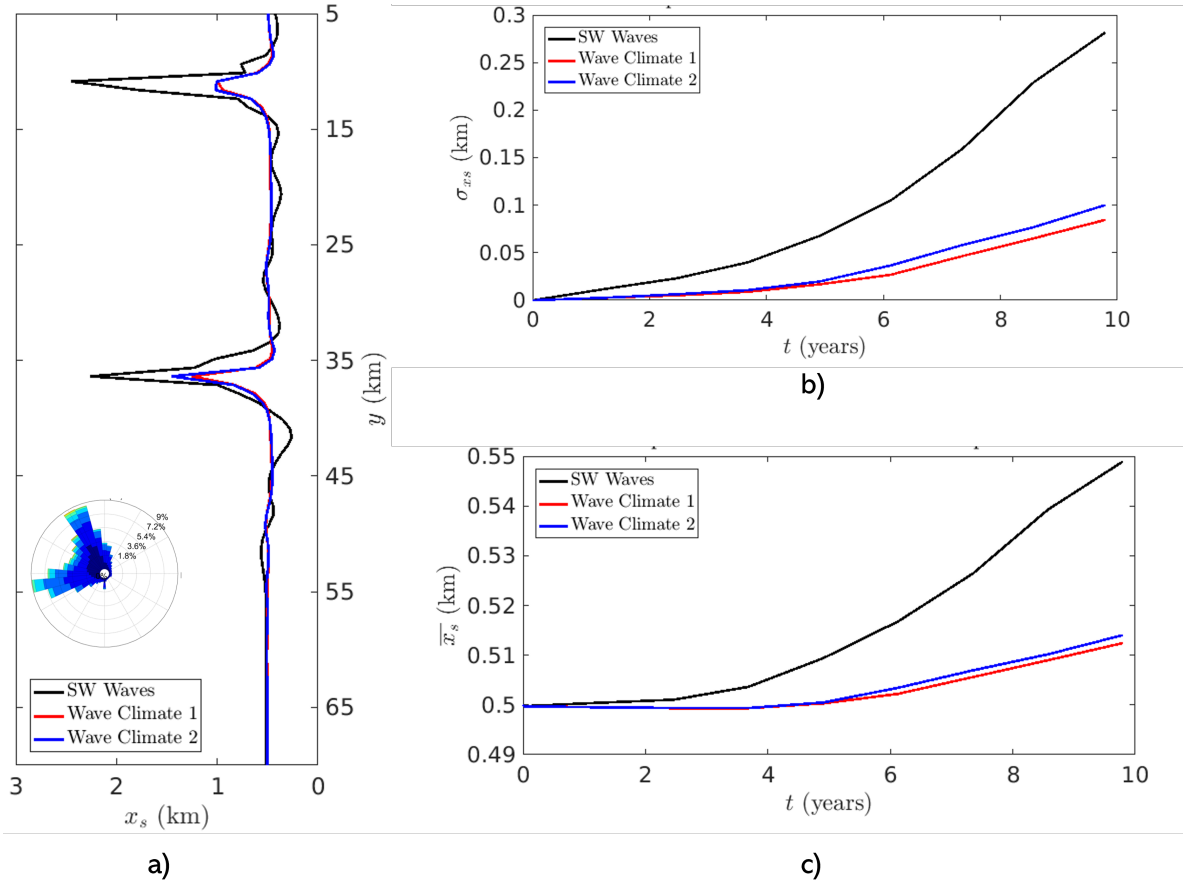

Figure 3.14: a) Shoreline position x_s at ten years is plotted against the longshore position for default ridges forced by constant south-western waves (black line), Wave climate realization 1 (red line), and wave climate realization 2 (blue line) (RQ3, see Experiment 5 in Table 2.2). b) Shoreline undulations amplitude $\sigma_{x's}$ is plotted against time for constant south-western waves (black line), Wave climate realization 1 (red line), and wave climate realization 2 (blue line). c) As b), but the mean shoreline position $\overline{x_s}$ is plotted against time.

4 | Discussion

4.1 Physical interpretation

This research expands our understanding of the impact of a bi-directional wave climate and almost shore parallel, onshore-located sand ridges to decadal shoreline evolution in the presence of significant tides. The results show that the presence of such ridges results in accumulation and erosion hotspots with a fixed location which depends on the hydrodynamic conditions and characteristics of the ridge and are much more prominent in magnitude (factor 10) than the free shoreline sand waves that are observed when no ridges are present. Figure 4.1 depicts the physical mechanism behind this.

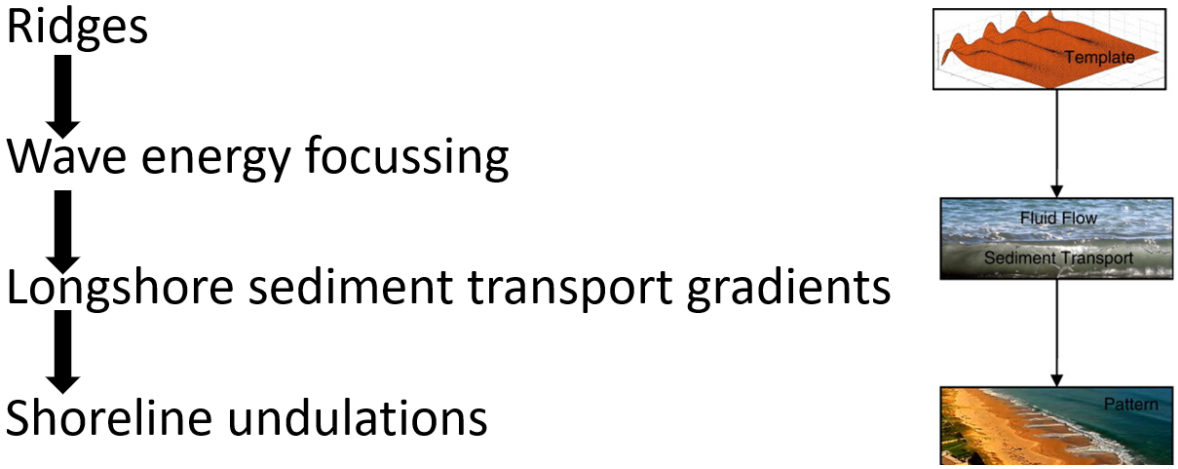

Figure 4.1: Schematic of the physical mechanism responsible for the large shoreline undulations observed in the presence of shoreface-connected ridges as simulated in this study. The morphological template leads to a hydrodynamic template by focusing and defoccusing of waves. This leads to gradients in littoral drift, leading to shore evolution and large shoreline undulations. Adapted from Coco and Murray (2007).

The presence of ridges on the shelf result in a hydrodynamic forcing template at the boundary of the nearshore zone. Figure 4.2 shows the wave energy density ($E = \frac{1}{16}\rho g H_s^2$), normalized with $E_0 = 3 \cdot 10^3$ J/m^2 in the eastern part of the shelf and the nearshore zone for simulations without ridges (Figure 4.2a), with ridges present and waves from the south-west (Figure 4.2b), and with ridges present and waves from the north-west (Figure 4.2c). In this figure, light colors indicate areas with relatively high wave energy, and dark colors indicate areas with relatively

low wave energy. The wave energy is distributed fairly homogeneously when no ridges are present. When ridges are present, however, wave energy hotspots can be found along the crests of the ridges, which are maintained in the nearshore zone. Hence, the ridges on the shelf act as a forcing template for the evolution of the adjacent shoreline by creating hotspots of low and wave energy density along this shoreline.

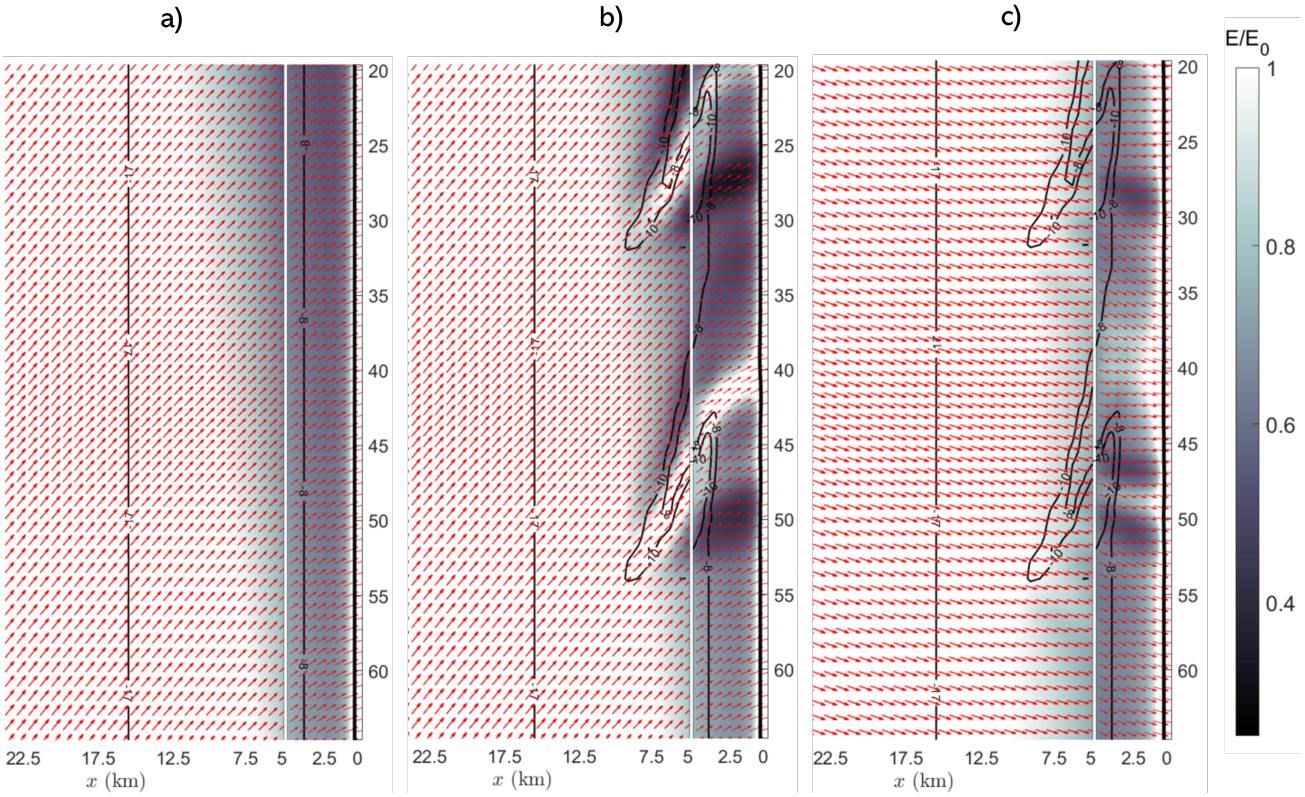

Figure 4.2: a) Greyplot showing the spatial distribution of the wave energy density $E = \frac{1}{16}\rho g H_s$ for the default conditions when ridges are absent at $t = 1$ years in the shelf and nearshore zone, for waves from the south-west. The intensity is normalized (E/E_0) with a reference magnitude of $E_0 = 3 \cdot 10^3$ J/m^2, so that dark and white colors represent areas of minimal and maximal wave energy density, respectively. The red arrows denote the group velocity vector $\mathbf{c_g}$. Black lines indicate the bed-level contours. b) As a), but with ridges present. c) As b), but for waves from the northwest.

The results show that the presence of the ridges causes longshore variation in wave forcing by wave focussing/defocussing that is not observed when the ridges are absent. This gives rise to gradients in longshore transport, which lead to erosion and accretion in specific spots related to the position of the shoreface-connected ridges. These locations are consistent across the experiments and in time, and free shoreline undulations are not observed on the same scale. This template is stronger for the waves from the southwest and less for the northwest waves. In all experiments incorporating ridges, the longshore lengthscales of the shoreline undulations are similar to the longshore lengthscale of the ridges (~ 25 km). The magnitude of erosion and accumulation hotspots is largest when the ridges' crest orientation aligns with the direction of incoming waves and for ridges located close to the shoreline. Under time-varying

wave conditions, different wave angles induce opposite patterns in the corresponding sediment transport gradients, limiting the growth of shoreline undulations. The observed focussing of wave energy aligns with the results of Nnafie et al. (2021).

Tides

This research incorporated the effect of tides on wave propagation on the shelf but not in the nearshore zone. On the shelf, tides influence waves mainly through the interaction of tidal currents and waves. These currents vary in time and space. Waves traveling on a current and waves traveling over a variable wave field are affected. When waves propagate on a current, one must consider two frames of reference: a moving or relative frame of reference, which travels at the speed of the current, and a stationary or absolute frame of reference. In the relative frame, the wave equations still hold. However, the wavelength remains the same in the absolute frame despite the wave being moved at a different speed. This is because the dispersion equation determines the wavelength in the relative frame. As a result, the absolute and relative wave periods differ. On the other hand, if waves propagating in still water encounter a current, alterations in both the wave height and wavelength will transpire. This happens because the absolute wave period must remain the same for waves to be conserved as they move from one region to another. Another instance of the interaction between waves and currents is known as current refraction, which occurs when a wave travels at an oblique angle with a variation in the current field (Holthuijsen, 2007). As the ridges on the shelf significantly influence the flow field, see Figure 3.2, which influences the wave field and, therefore, the boundary conditions of the nearshore zone. In the absence of tides on the shelf, the growth of shoreline undulations is amplified; see Figure 4.3a (Nnafie et al., 2021).

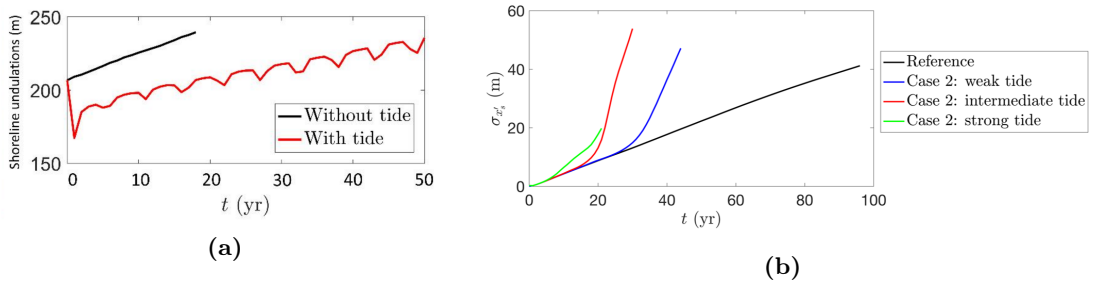

(a) **(b)**

Figure 4.3: a) Growth of shoreline undulations in the presence of tides (red line) and when tides are absent (black line), as modeled and presented by Nnafie et al. (2021). b) Growth of shoreline undulations in the presence of weak (blue line), intermediate (red line), and strong tides (green line), compared to no tides (black line), for standalone simulations of the nearshore zone similar to the reference case in this study, for constant south-western waves. Modelled and presented by Nnafie et al. (2023).

Furthermore, tides are not included in the nearshore zone. For standalone simulations of the nearshore zone similar to the reference case in this study with constant south-western waves, Nnafie et al. (2023) showed in a pilot study that the effect of tides might be of importance in the development of shoreline undulations, see Figure 4.3b. Especially in the case of strong tides (tidally induced sediment transport of $6 \cdot 10^{-4}$ m^3/s/m at the offshore boundary), the

effect of tides in de deeper zones of the domain is significant.

Strong tides on the shelf lead to the formation of tidal sand ridges, which are large bedforms of similar size to the shoreface-connected ridges discussed here (Nnafie et al., 2020). The Belgian coast prototype system features tidal sand ridges; see Figure 1.7. Their orientation aligns approximately with north-north-west, so focusing of waves from that direction is strongest. The SFCR in this study align with the geographical south-west, enhancing shoreline evolution strongest for waves from that direction. The combined effect of these two different sand ridges is relevant, as both have been shown to influence the wave field and shoreline development significantly. As tidal sand ridges affect wave focusing/defocusing in a similar way as the shoreface-connected ridges in this study, but in different (opposing) directions and locations (Nnafie et al., 2021), their effect would likely partially cancel out the effect of the shoreface-connected ridges, and therefore decrease the size of shoreline undulations.

4.2 Comparison with observations

Qualitatively, the results line up with the observations. The erosion hotspots line up with the location of the trough of the SFCR, and accumulation hotspots are found at the location of the ridge. This is similar to the Belgian coast prototype shelf-shoreline system. This system contains three shoreface connected ridges; see Figure 1.7. The southern/western shoreface connected ridges, the Trapegeer-Broersbank complex at Koksijde, is thought to form a natural sand engine that feeds a significant portion of the Belgian west coast (Verwaest et al., 2022b). Evidence of this is seen in the coastline, which features a seaward protrusion of several hundred meters between Koksijde-Bad and Oostduinkerke-Bad (Figure 4.4).

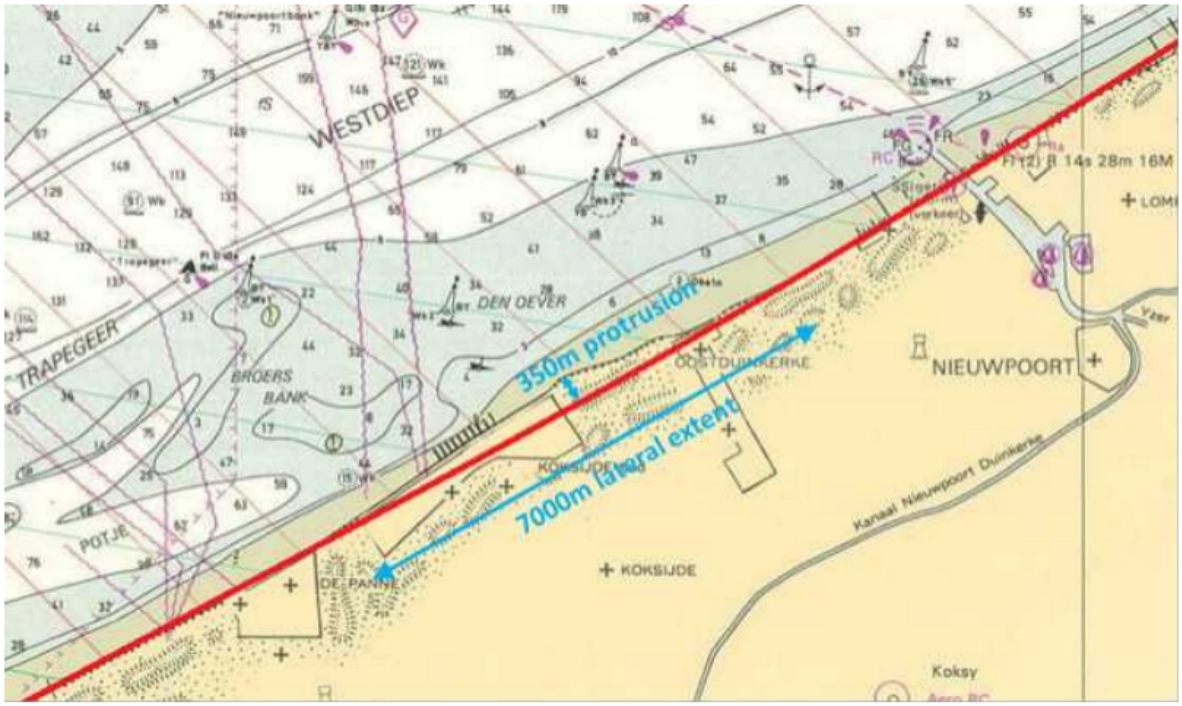

Figure 4.4: A hydrographic map of the study area. The map shows a headland at Sint-André that protrudes 350 m. Adopted from Verwaest et al. (2020)

The estimated magnitude of shoreward flux from the ridges is $\sim 85,000$ m3/year (Verwaest et al., 2020, 2022b,a; Houthuys et al., 2021), which is larger with the cross-shore transport observed in these simulations. The cross-shore integrated alongshore sediment transport (integrated between the depth of closure $D_c = 8$ m and the shoreline x_s) is of a magnitude of $\sim 3 \cdot 10^5$ m^3/ year, which agrees with observations in the Belgium nearshore zone (Verwaest et al., 2011). However, it is important to note that recent human activities such as beach nourishment, the construction of groins and harbors, etc. may have had an impact on the shape of the Belgian shoreline in the past few decades (Deronde et al., 2008), complicating the comparison between the findings of the model and actual observations.
The shoreline undulations in this research far exceed the magnitude of observed undulation for both constant and varying waves. The latter is particularly surprising, as the variation in wave direction has been demonstrated to yield realistic results for tidal sand ridges (Nnafie et al., 2021). Suppose the large progradation area is not taken into account. In that case, using a synthetic wave climate leads to forming a relatively unvarying shoreline, which aligns with the actual observations.

Similar to the Belgian coast, persistent shoreline undulations are lacking along the Dutch coast despite SFCR on the adjacent shelf Ruessink and Jeuken (2002). While large-scale shoreline sand waves have been observed along the central Dutch coast, they are not persistent and have shorter lifetimes relative to the time scales of the ridges. These shoreline sand waves are highly dynamic and have longshore migration rates of tens to hundreds of meters per year. Their formation is likely due to high-angle wave instability, which cannot be correlated with the presence of almost static ridges (Falqués, 2006). These shoreline sand waves are also present

in these simulations, especially visible in the reference case where no ridges are present. When ridges are present, the shoreline undulations caused by wave focussing of the ridges overshadow the shoreline sand waves.

The persistent shoreline undulations found in this study are in line with the hypothesis of Safak et al. (2017) and the results of Nnafie et al. (2021) for the shoreline undulations on Fire Island due to the presence of shoreface connected ridges. With the above restrictions concerning the conclusions, shoreface-connected sand ridges will likely significantly impact coastline evolution. The results are for shore-oblique, offshore located ridges as present at Fire Island in a microtidal, unimodal waveclimate.

Considering the discussed influence of ridge distance to the coast, ridge orientation, wave angle, and wave angle variation on the evolution of shoreline undulations, the two systems can be compared. For more shore-parallel ridges, smaller undulations are expected for the considered wave conditions. The strongest shoreline undulations are expected for a distance close to the coast. The findings suggest that wave climates characterized by considerable variability in wave angles, such as the wave climate of the Belgium coast, are likely to result in weaker shoreline undulations in comparison to wave climates with a smaller variability in wave angles, such as the wave climate of Fire Island.

4.3 Model artefacts

Another source of sediment transport is identified in the results, which expresses itself in a shoreward-driven cross-shore sediment flux in the deeper part of the nearshore zone, the transition zone. This mechanism becomes increasingly more important after ten years of simulation. The ridges within the nearshore zone create a nearshore bathymetry that diverts from the equilibrium Dean profile. Due to the assumption that the bathymetry adjusts to this equilibrium profile on longer timescales, a cross-shore sediment flux is attributed to smooth out such disturbances. However, the method of Nnafie et al. (2021) incorporates yearly bed level coupling in the transition zone, which sets the bathymetry in the transition zone as an average of the shelf bathymetry and the nearshore bathymetry. In a morphodynamic shelf domain, changes in the nearshore area affect changes on the shelf and vice versa. This study, however, incorporates a morphostatic shelf. Therefore, the bed level coupling re-establishes the disturbances that the nearshore model tends to flatten out, and each iteration imprints a bit more ridge in the nearshore bathymetry. The consequences are large as it results in the enhanced growth of coastline undulations, especially of the progradation areas. In Figure 4.5, the effect of bed coupling timestep can be seen.

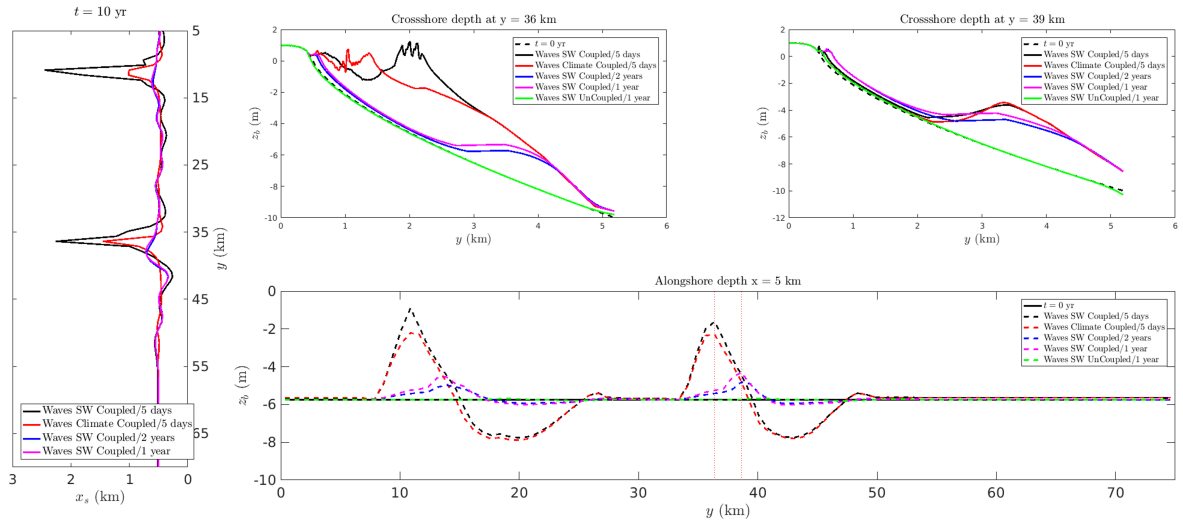

Figure 4.5: Overview of the shoreline (left) and nearshore bathymetry z_b at different locations after ten years of simulation for different bed level coupling timesteps (5 days, 1 year, 2 years, no coupling). Nearshore bathymetry. Cross-shore transects at y = 36 km (upper central) and y = 39 km (upper right), near the southern ridge, and an alongshore transect at x = 2.6 km (lower right), the shoreward end of the transition zone, of nearshore bed level z_b are shown.

This shows that the method of Nnafie et al. (2021) for modeling shoreline development leads to problems in the presence of significant ridges nearshore of the outer boundary of the coupling zone, in combination with a morphostatic shelf bathymetry. Therefore, proposed is to couple the shelf and nearshore bed only at the initiation. From that point, the development of the nearshore is only influenced by the incoming waves at the offshore boundary and the bathymetry of the nearshore zone. A pilot experiment, referred to as "Initiated" from this point onward, is set up to explore this approach. The results are shown in Figure 4.6, with settings like the Default experiment with ridges but bed level coupled only once at t=0. The results show that the Initiated approach yields far more steady nearshore development. After ten years of simulation time, the results of the Initiated approach are similar to the coupled experiment, where the progradation part of the shoreline undulations of the Default experiment are somewhat larger. The evolution rapidly diverts between the cases from this point. The shoreline undulations in the Default experiment start growing exponentially, with that, the mean shoreline position until the maximum seaward extent of the shoreline has reached the transition zone. For the Initiated approach, the shoreline undulations continue to grow steadily, extending seaward to a maximum of $\sim$ 1 km. Note that while the large protrusion area is three times smaller after 50 years for the Initiated approach than for the Coupled approach, the relative locations of the shoreline undulations concerning the location of the ridge are (almost) identical.

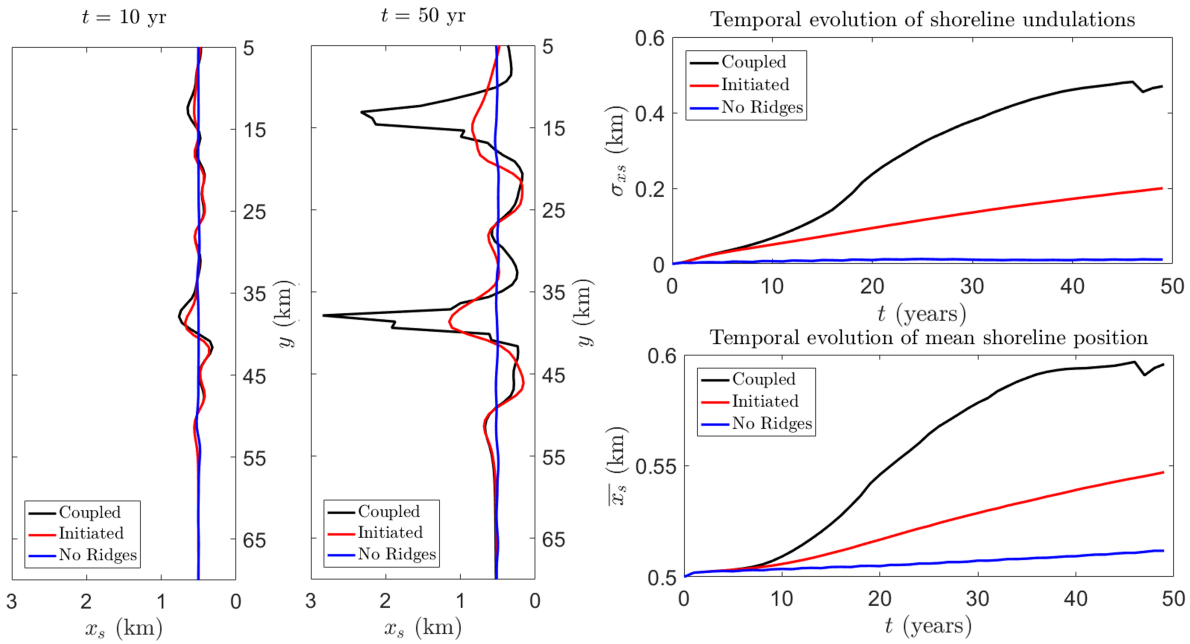

Figure 4.6: Results for the default case with regular bed level coupling (Coupled), the pilot experiment with coupling at initiation (Initiated), and regular case without ridges (No Ridges). Shoreline position x_s is shown for t=10 years and t = 50 years on the left. Temporal evolution of shoreline undulations $\sigma_{x's}$ and mean shoreline position $\overline{x_s}$ are shown respectively, upper right and lower right.

Furthermore, this approach prevents importing large amounts of sediment due to bed coupling. While the bed level gradients in the transition zone still import sediment, the total sediment imported is five times smaller than the coupled case. In contrast with the bed coupling timestep, the wave coupling timestep has no significant influence.

The results indicate two types of forcing templates, a hydrodynamic forcing template that influences the evolution of the shoreline through variation in longshore sediment transport and a forcing template due to a bathymetry that deviates from the assumed equilibrium profile. The hydrodynamic forcing template has a physical basis and applies to our conclusions. This limits the part of the results that are relevant for this research, as the acceleration of the development of the shoreline undulations, and in particular, the accumulation zone, after $\sim$ 15 year is more due to the effect of frequent bed-coupling, disturbance of the equilibrium profile and shoreline curvature than due to the hydrodynamic template.

Future research involving a similar coupled shelf-shoreline model should be aware of the effect of bed level coupling as discussed above. Furthermore, ridges in the nearshore zone disturb the equilibrium profile, causing a cross-shore sediment flux. Therefore, an alternative approach is required to incorporate bed-level variation induced by the presence of ridges in the nearshore zone without creating additional sediment fluxes. Additionally, the effect of more realistic wave forcing can be explored. In this study, a wave climate is used that consists of randomly varying conditions. In reality, however, wave conditions are often not completely random but have some correlation with the conditions of the period before (Holthuijsen, 2007).

5 | Conclusions

Almost shore-parallel, onshore-located, shoreface-connected sand ridges are a forcing template for the evolution of shoreline undulations. Their presence leads to a local decrease in tidal current magnitude, creating longshore variation in sediment transport rates by focusing and defocusing wave energy. Accumulation (erosional) hotspots form near crests (troughs). The longshore extent of these shoreline undulations is similar to the longshore extent of the ridges. This effect is strongest for ridges with crest orientations that align with the direction of the incoming waves and weaker for ridges with crest orientations that align less with the direction of incoming waves. Specifically, the hydrodynamic template of more shore parallel ridges causes more minor cross-shore undulations. Ridge distance impacts the shoreline by influencing the longshore width of the wave energy hotspots and the angle at which these waves incide on the shore. The closer the ridges are to the shore and the larger the angle with the coast, the stronger these hotspots are. Locations of these hotspots vary for different offshore distances, ridge orientations, and wave directions. Specifically, more offshore ridges have hotspots that are shifted in the direction of the longshore current and littoral drift (north for south-western waves). The same up-drift shift occurs for less-shore parallel ridges compared to more shore parallel ridges and for waves more aligned with the ridges' crests than the ridges' troughs. Wave variation leads to undulations that are smaller than for constant waves, while the location of accumulation and erosional hotspots are not influenced. The results qualitatively agree with observations, although the growth rate and absolute magnitude exceed realistic conditions.

Bibliography

Arriaga, J., Rutten, J., Ribas, F., Falqués, A., and Ruessink, G. (2017). Modeling the long-term diffusion and feeding capability of a mega-nourishment. *Coastal Engineering*, 121:1–13.

Ashton, A., Murray, A. B., and Arnoult, O. (2001). Formation of coastline features by large-scale instabilities induced by high-angle waves. *Nature*, 414(6861):296–300.

Ashton, A. D. and Murray, A. (2006). High-angle wave instability and emergent shoreline shapes: 1. modeling of sand waves, flying spits, and capes. *J. Geophys. Res. Earth Surf.*, 111:1–19.

Battjes, J. A. and Janssen, J. (1978). Energy loss and set-up due to breaking of random waves. In *Coastal engineering 1978*, pages 569–587.

Bindels, M. (2020). The impact of sea level rise on tides, waves and tidal sand ridges in the north sea. Master's thesis.

Booij, N. and Holthuijsen, L. H. (1987). Propagation of ocean waves in discrete spectral wave models. *Journal of Computational Physics*, 68(2):307–326.

Bosboom, J. and Stive, M. J. (2021). *Coastal Dynamics*. Delft University of Technology.

Castelle, B., Ruessink, G. B., Bonneton, P., Marieu, V., Bruneau, N., and Price, T. D. (2010). Coupling mechanisms in double sandbar systems. part 1: Patterns and physical explanation. *Earth Surface Processes and Landforms*, 35(4):476–486.

Coco, G. and Murray, A. B. (2007). Patterns in the sand: From forcing templates to self-organization. *Geomorphology*, 91(3-4):271–290.

Deltares (2019). User manual delft3d-flow: Simulation of multi-dimensional hydrodynamic flows and transport phenomena, including sediments. Technical Report Version 3.15, SNV revision: 60015, Deltares, Delft, The Netherlands.

Deronde, B., Houthuys, R., Henriet, J.-P., and Lancker, V. V. (2008). Monitoring of the sediment dynamics along a sandy shoreline by means of airborne hyperspectral remote sensing and lidar: a case study in belgium. *Earth Surface Processes and Landforms: the Journal of the British Geomorphological Research Group*, 33(2):280–294.

Dyer, K. R. and Huntley, D. A. (1999). The origin, classification and modelling of sand banks and ridges. *Continental shelf research*, 19(10):1285–1330.

Elko, N., Feddersen, F., Foster, D., Hapke, C., McNinch, J., Mulligan, R., Özkan-Haller, H. T., Plant, N., and Raubenheimer, B. (2015). The future of nearshore processes research. *Shore Beach*, 83(1):13.

Falqués, A. (2006). Wave driven alongshore sediment transport and stability of the dutch coastline. *Coastal Engineering*, 53(2-3):243–254.

Falqués, A. and Calvete, D. (2005). Large-scale dynamics of sandy coastlines: Diffusivity and instability. *Journal of Geophysical Research: Oceans*, 110(C3).

Falqués, A., Ribas, F., Idier, D., and Arriaga, J. (2017). Formation mechanisms for self-organized kilometer-scale shoreline sand waves. *Journal of Geophysical Research: Earth Surface*, 122(5):1121–1138.

Hamon-Kerivel, K., Cooper, A., Jackson, D., Sedrati, M., and Guisado Pintado, E. (2020). Shoreface mesoscale morphodynamics: A review. *Earth-Science Reviews*, 209:103330.

Hanson, H. (1989). Genesis: a generalized shoreline change numerical model. *Journal of Coastal research*, pages 1–27.

Hasselmann, K., Barnett, T., Bouws, E., Carlson, H., Cartwright, D., Enke, K., and Kruseman, P. (1973). Measurements of wind-wave growth and swell decay during the joint north sea wave project (jonswap). *Deutschen Hydrographischen Zeitschrift, Reihe A*, 12(A8):1–95.

Holthuijsen, L. H. (2007). *Waves in oceanic and coastal waters*. Cambridge University Press.

Houthuys, R., Vos, G., Dan, D., and Verwaest, T. (2021). Long-term morphological evolution of the flemish coast: Holocene, late middle ages to present. FHR reports 14_023_1, Flanders Hydraulics Research.

Idier, D., Falqués, A., Ruessink, G., and Garnier, R. (2011). Shoreline instability under low-angle wave incidence. *Journal of Geophysical Research: Earth Surface*, 116(F4):F04031.

Komar, P. D. (1998). *Beach processes and sedimentation*. Prentice Hall, Englewood Cliffs, NJ, 2 edition.

Komen, G., Hasselmann, S., and Hasselmann, K. (1984). On the existence of a fully developed wind-sea spectrum. *Journal of physical oceanography*, 14(8):1271–1285.

Lesser, G. R., Roelvink, J. v., van Kester, J. T. M., and Stelling, G. (2004). Development and validation of a three-dimensional morphological model. *Coastal engineering*, 51(8-9):883–915.

Longuet-Higgins, M. and Stewart, R. (1964). Radiation stresses in water waves; with applications a physical discussion. *Deep-Sea Research*, 11:529–562.

Nnafie, A. (2014). *Formation and long-term evolution of shoreface-connected sand ridges: modeling the effects of sand extraction and sea level rise*. PhD thesis, Utrecht University.

Nnafie, A., de Swart, H., Falqués, A., and Verwaest, T. (2023). Shoreline evolution on decadal time scales: role of tides. In *Abstracts of Oral Presentations, NCK Book of abstracts*, The Netherlands. Conference abstract.

Nnafie, A., de Swart, H. E., Falqués, A., and Calvete, D. (2021). Long-term morphodynamics of a coupled shelf-shoreline system forced by waves and tides, a model approach. *Journal of Geophysical Research: Earth Surface*, 126(12):e2021JF006315.

Nnafie, A., Wolf, T., and de Swart, H. (2020). Tidal sand ridges on the shelf: A numerical study of their natural morphodynamic evolution and response to interventions. *Continental Shelf Research*, 205:104195.

Pelnard-Considere, R. (1956). Essai de theorie de l'evolutio des form de rivage en plage de sable et de galets. In *4th Journees de l'Hydaulique, Les Energies de la Mer*, volume No. 1, pages 289–298.

Pickering, M., Wells, N., Horsburgh, K., and Green, J. (2012). The impact on the european shelf tides by future sea-level rise. *Continental Shelf Research*, 35:1–15.

Pörtner, H.-O., Roberts, D. C., Poloczanska, E., Mintenbeck, K., Tignor, M., Alegría, A., Craig, M., Langsdorf, S., Löschke, S., Möller, V., et al. (2022). Ipcc, 2022: Chapter 4.

Ribas, F., Falqu'es, A., de Swart, H., Dodd, N., Garnier, R., and Calvete, D. (2015). Understanding coastal morphodynamic patterns from depth-averaged sediment concentration. *Reviews of Geophysics*, 53(2):421–466.

Roelvink, J. A. and Walstra, D.-J. (2004). Keeping it simple by using complex models. *Advances in Hydro-science and Engineering*, 6:1–11.

Roest, L. W. M. (2022). Nourishment efficiency along the belgian coast. *VLIZ Special Publication*, (89):56–57.

Ruessink, B. and Jeuken, M. (2002). Dunefoot dynamics along the dutch coast. *Earth Surface Processes and Landforms: The Journal of the British Geomorphological Research Group*, 27(10):1043–1056.

Safak, I., List, J. H., Warner, J. C., and Schwab, W. C. (2017). Persistent shoreline shape induced from offshore geologic framework: Effects of shoreface connected ridges. *Journal of Geophysical Research: Oceans*, 122(11):8721–8738.

Schwab, W. C., Thieler, E. R., Allen, J. R., Foster, D. S., Swift, B. A., and Denny, J. F. (2000). Influence of inner-continental shelf geologic framework on the evolution and behavior of the barrier-island system between fire island inlet and shinnecock inlet, long island, new york. *Journal of Coastal Research*, pages 408–422.

Soulsby, R. L., Hamm, L., Klopman, G., Myrhaug, D., Simons, R., and Thomas, G. (1993). Wave-current interaction within and outside the bottom boundary layer. *Coastal engineering*, 21(1-3):41–69.

Szmytkiewicz, M., Biegowski, J., Kaczmarek, L. M., Okroj, T., Ostrowski, R., Pruszak, Z., Różyńsky, G., and Skaja, M. (2000). Coastline changes nearby harbour structures: comparative analysis of one-line models versus field data. *Coastal Engineering*, 40(2):119–139.

Tao, J., Wang, Z. B., Zhou, Z., Xu, F., Zhang, C., and Stive, M. J. (2019). A morphodynamic modeling study on the formation of the large-scale radial sand ridges in the southern yellow sea. *Journal of Geophysical Research: Earth Surface*, 124(7):1742–1761.

Tonnon, P. K., Huisman, B. J., Stam, G. N., and van Rijn, L. C. (2018). Numerical modelling of erosion rates, life span and maintenance volumes of mega nourishments. *Coastal Engineering*, 131:51–69.

van den Berg, N., Falqués, A., and Ribas, F. (2011). Long-term evolution of nourished beaches under high angle wave conditions. *Journal of Marine Systems*, 88:102–112.

Van den Berg, N., Falqués, A., and Ribas, F. (2012). Modeling large scale shoreline sand waves under oblique wave incidence. *Journal of Geophysical Research: Earth Surface*, 117(F3).

Verwaest, T., Delgado, R., Janssens, J., and Reyns, J. (2011). Longshore sediment transport along the belgian coast. In *The proceedings of the coastal sediments 2011: In 3 volumes*, pages 1528–1538. World Scientific.

Verwaest, T., Dujardin, A., Montreuil, A.-L., and Trouw, K. (2022a). Understanding coastal resilience of the belgian west coast. *Water*. Submitted.

Verwaest, T., Houthuys, R., and Dan, S. (2022b). Shoreface connected ridges as natural sand engines for coastline preservation. In *Book of Abstracts*.

Verwaest, T., Houthuys, R., Roest, B., Dan, S., and Montreuil, A.-L. (2020). A coastline perturbation caused by natural feeding from a shoreface-connected ridge (headland sint-andré, belgium). In Malvárez, G. and Navas, F., editors, *Global Coastal Issues of 2020 Malvárez and Navas*, pages 701–705, Coconut Creek, FL. Journal of Coastal Research, Special Issue, No. 95.

A | Cross-shore profile formulations

$$H(x) = \begin{cases} -b\Big(1 - e^{\frac{\beta(x-x_{s0})}{b}}\Big) & \text{if} \quad 0 \leq x \leq x_{s0}, \\ \frac{3}{2}\beta\alpha^{\frac{1}{3}}\Big[(x - x_{s0} + \alpha)^{2/3} - \alpha^{2/3}\Big] & \text{if} \quad x_{s0} \leq x \leq x_2, \\ \frac{H_2 - H_1}{x_2 - x_L}(x_2 - x_L) + H_1 & \text{if} \quad x_2 \leq x \leq x_L. \end{cases} \tag{A.1}$$

$$H(x_2) = \frac{3}{2}\beta\alpha^{\frac{1}{3}}\Big[(x - x_{s0} + \alpha)^{2/3} - \alpha^{2/3}\Big] = H_1 \tag{A.2}$$

B | Parameters in the the nearshore model

The angle ϕ is determined using the relation

$$\sin\phi = \frac{\frac{\partial z_{b1}}{\partial y}}{\sqrt{(\frac{\partial z_{b1}}{\partial x})^2 + (\frac{\partial z_{b1}}{\partial y})^2}}. \tag{B.1}$$

It is scaled by a power of the significant wave height at the breaker point xb.

$$-\gamma_C = \nu_b g^{1/2} \gamma_b^{1/6} H_{s,b}^{11/6} L_1^{-1/3} \Psi. \tag{B.2}$$

In the equation, ν_b is a dimensionless parameter and Ψ is a function of the cross-shore distribution of wave orbital motion. This function has a maximum at the shoreline, where $\Psi = 1$ at $x = x_s$ and decreases to zero in both the offshore $x < x_s$ and onshore $x > x_s$ directions. For wet cells where $zb1 < 0$, the following expression for Ψ is used as a function of $zb1$:

$$\Psi(z_b) = \frac{1 + b + \tanh[\frac{\alpha D_c + z_{b1}}{L_d}]}{1 + b + \tanh[\frac{\alpha D_c}{L_d}]} \tag{B.3}$$

Here, α and b are non-dimensional constants, D_c is the depth of closure and L_d is the decay distance, which is set to $L_d = 0.5\alpha D_c$. In the dry cells $zb1 > 0$, the function decays in the onshore direction according to the following expression:

$$\Psi(x - x_s) = \exp\left[-(\frac{x - x_s}{L_2})^4\right] \tag{B.4}$$

where $x - x_s$ is the distance to the shoreline. The width of the swash-zone L_2 controls the decay distance.

C | Formulation for the shape of the artificial ridges

The cross-ridge shape is formulated as

$$z_{sfcr}(x,y) = -(A_r \sin(2\pi((y_f - Y_b)/Lr) + 0.2A_r \sin(4\pi((y_f - Y_b)/Lr + 1.75\pi)\tanh(8.4/x_b)))), \tag{C.1}$$

where A_r is the ridge amplitude in meters, y_f is the across-ridge coordinate, L_r is the (cross-ridge) wavelength, x_f is the along-ridge coordinate, and b is the along-ridge scaling length. Furthermore, SFCR are slightly curved in the along-ridge direction, especially near the tip. This tip-curvature is obtained by setting reference distance Y_b as a function of x_f,

$$Y_b = y_{ref}(1 + 0.1\tanh(s_f/b(1 - x_f))) + (1 - \max(1 + 0.1\tanh(s_f/b(1 - x_f)))), \tag{C.2}$$

where s_f is an arbitrary factor that determines the tip-curvature.